JOURNAL OF GEOPHYSICAL RESEARCH, VOL. 113, C02S07, doi:10.1029/2007JC004257, 2008

Trends in the sea ice cover using enhanced and compatible AMSR-E, SSM/I, and SMMR data

Josefino C. Comiso[1] and Fumihiko Nishio[2]

Received 1 April 2007; revised 26 August 2007; accepted 24 December 2007; published 22 February 2008.

[1] Arguably, the most remarkable manifestation of change in the polar regions is the rapid decline in the Arctic perennial ice cover. Changes in the global sea ice cover, however, have been more modest, being only slightly negative in the Northern Hemisphere and even slightly positive in the Southern Hemisphere, the significance of which has not been adequately assessed because of unknown errors in the satellite historical data. Recent Advanced Microwave Scanning Radiometer (AMSR-E) high-resolution data are used as the baseline for generating an enhanced sea ice data set used in this study. Brightness temperature data from historical Special Scanning Microwave Imager (SSM/I) and Scanning Multichannel Microwave Radiometer (SMMR) sensors were normalized to be consistent with those from AMSR-E, and sea ice parameters were derived from all three data sets using the same algorithm for optimum consistency and accuracy. A small bias in sea ice extent is observed between AMSR-E and SSM/I data which, if uncorrected, causes an error of 0.62%/decade in the Arctic and 0.26%/decade in the Antarctic. Similar corrections are not needed in trend estimates of sea ice area. Biases due to seasonal changes in the accuracy of ice edge determinations, especially during melt periods, were also evaluated, and impacts on the trend results appear to be small. When updated to 2006, the trends in ice extent and area in the Arctic are now slightly more negative at -3.4 ± 0.2 and -4.0 ± 0.2% per decade, respectively, while the corresponding trends in the Antarctic remains slight but positive at 0.9 ± 0.2 and 1.7 ± 0.3% per decade.

Citation: Comiso, J. C., and F. Nishio (2008), Trends in the sea ice cover using enhanced and compatible AMSR-E, SSM/I, and SMMR data, *J. Geophys. Res.*, *113*, C02S07, doi:10.1029/2007JC004257.

1. Introduction

[2] Much of what we currently know about the large-scale variability of the global sea ice cover has been based on data provided by satellite passive microwave sensors [*Parkinson et al.*, 1999; *Bjorgo et al.*, 1997; *Zwally et al.*, 2002]. This capability for studying the sea ice cover has recently been improved considerably with the launch of the Advanced Microwave Scanning Radiometer in May 2002 on board the EOS-Aqua satellite (referred to as AMSR-E). The improvements of AMSR-E over the Special Scanning Microwave Imager (SSM/I), which has been the primary source of data since July 1987, include higher resolution at all frequencies, wider spectral range and wider swath width. In particular, AMSR-E has integrated field-of-views of 26 by 16 km and 14 by 10 km with its 18.7- and 36.5-GHz channels while the SSM/I has integrated field-of-views of 56 by 56 and 34 by 34 km with its 19.35- and 37.0-GHz channels, respectively. For the period from November 1978 to August 1987, similar data were provided by the Scanning Multichannel Microwave Radiometer (SMMR), which had field of views of 54 by 35 km and 28 by 18 km for its 18- and 37-GHz channels, respectively. The AMSR-E instrument scans conically with a swath width of 1450 km at an incidence angle of 55° while SSM/I scans similarly with a swath width of 1390 km at an incidence angle of 53.1°. The wider swath for AMSR has enabled almost complete coverage near the poles where data are usually missing owing to satellite inclination. Also, the higher spatial resolution of AMSR-E minimizes the uncertainties associated with the use of mixing algorithms to retrieve geophysical sea ice parameters.

[3] The polar regions are expected to provide early signals of a climate change primarily because of the "ice-albedo feedback" which is associated with changes in absorption of solar energy due to changes in the area covered by the highly reflective sea ice. Recent reports have indeed shown that the perennial ice cover in the Arctic has been declining at a rapid rate of about 10% per decade [*Comiso*, 2002; *Stroeve et al.*, 2004; *Comiso*, 2006]. While this has led to speculations of an ice free Arctic in summer within this century, hemispherical changes including those from seasons other than summer have been more modest at about 2 to 3% per decade [*Bjorgo et al.*, 1997; *Parkinson et al.*, 1999; *Serreze et al.*, 2000]. Moreover, in the Antarctic,

[1] Cryospheric Sciences Branch, NASA Goddard Space Flight Center, Greenbelt, Maryland, USA.
[2] Center for Environmental Remote Sensing, Chiba University, Chiba City, Japan.

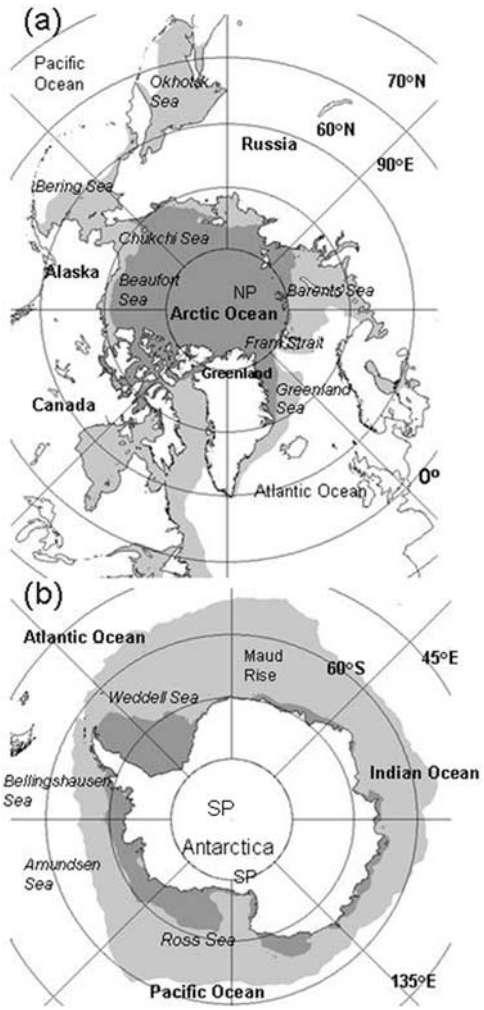

Figure 1. Location map for (a) the Northern Hemisphere and (b) the Southern Hemisphere. The dark and light shades of gray correspond to the climatological average of the ice cover during minimum and maximum extents, respectively.

the trends are also slight but in the opposite direction [*Cavalieri et al.*, 1997; *Zwally et al.*, 2002]. The significance of estimates in the trends, has not been fully evaluated because of unknown uncertainties in the parameters derived from historical satellite data. A key problem in analyzing long-term trends is that data from a number of different sensors have to be assembled together to make up the historical time series of satellite data we currently have. There are also known mismatches in calibration and resolution between sensors and there are no measurements (in situ or high-resolution satellite data) that can be used to assess how accurately the large-scale characteristics of the sea ice cover are represented by the historical passive microwave ice data.

[4] Among the specific objectives of this study are (1) to assess the merit of combining AMSR-E data with historical satellite data with a view of generating an enhanced and consistent sea ice data set suitable for time series studies; (2) to evaluate errors and biases associated with using such a combined data set for trend analysis; and (3) to provide updated and improved estimates of the trends in the sea ice cover. The primary tool we use is the AMSR-E data which provide similar coverage as historical data but has many advantages as described earlier. The AMSR-E ice algorithm has benefited from the availability of the Moderate Resolution Imaging Spectroradiometer (MODIS) on board the Aqua satellite that provides near-concurrent visible observations of the same surface during cloud free conditions. MODIS data have been utilized through comparative studies to optimize input parameters in the algorithms used to derive AMSR-E sea ice data [e.g., *Comiso*, 2004]. Other data sets can also be used for the same purpose, such as high-resolution Synthetic Aperture Radar (SAR) and Landsat data, but spatial and temporal coverage from these types of sensors are limited and not coincident. With considerable improvement in resolution, AMSR-E data are expected to provide a more accurate characterization of the sea ice cover than currently available historical passive microwave data. In the long run, data from AMSR-E and similar systems will become the core of sea ice variability studies and it is important that we evaluate its potential as well as its limitations in the study of long-term trends in the sea ice cover.

2. Consistent Retrieval of Sea Ice Concentrations

[5] The spatial distributions of sea ice in the two hemispheres are quite different in that sea ice is surrounded by continental landmasses in the Northern Hemisphere and is generally located at higher latitude while in the Southern Hemisphere, it is sea ice that surrounds Antarctica and may be found at lower latitudes (Figure 1). In the winter, the Arctic basin is basically covered by consolidated ice that is more confined, thicker and colder than sea ice in the Antarctic. In the Arctic, a large fraction of the ice floes survive the summer melt and can be as old as 7 years [*Colony and Thorndike*, 1985], while in the Antarctic, it is rarely the case that an ice floe is older than 2 years. The reason for younger Antarctic ice is that the ice that survives the summer melt in the region usually gets flushed out of the original location and to the warmer waters by strong ocean currents (e.g., Weddell gyre) during autumn and winter. Also, the impact of divergence on Antarctic sea ice is stronger than in the Arctic because of the lack of an outer boundary in the former, causing more and larger leads and basically more new ice than in the latter.

[6] Sea ice is an inhomogeneous material consisting not only of ice but also of brine, air pockets, and other impurities, the relative percentages of which varies spatially depending on formation conditions and history of the ice [*Weeks and Ackley*, 1986; *Tucker et al.*, 1992; *Eicken et al.*, 1991]. We now know that these inhomogeneities affect the dielectric properties of sea ice in the two regions and hence the emissivity or radiative characteristics [*Vant et al.*, 1974; *Grenfell*, 1992]. Hemispherical differences in environmental conditions thus affect the radiative signature of sea ice in the Arctic making it generally different from the Antarctic. This results in differences in the brightness temperatures as measured by passive microwave sensors, especially for consolidated ice, making it necessary to use different input data for the sea ice algorithms used to retrieve sea ice parameters in the two hemispheres [*Comiso et al.*, 2003; *Comiso*, 2004].

[7] Among the most basic geophysical cryospheric parameters that are derived from passive microwave data is sea ice concentration. Sea ice concentration, C_I, has been defined as the percentage fraction of sea ice within the field of view of the sensor. Such percentage has been calculated using a linear mixing equation [*Zwally et al.*, 1983] given by

$$T_B = T_I C_I + T_O(1 - C_I), \quad (1)$$

where T_B is the brightness temperature observed by the sensor while T_I and T_O are the brightness temperature of sea ice and open water, respectively, in the region of observation. Sea ice algorithms are formulated with the goal of estimating T_I and T_O within the satellite footprint as accurately as possible. In the Rayleigh-Jeans' approximation, the brightness temperature of a surface is equal to its effective emissivity multiplied by the physical temperature of the emitting surface. Equation (1) suggests that data from one channel is all that is required if the emissivities of ice and water are unique and the surface temperature is known. However, this is not the case because of known spatial and temporal variability of emissivity and temperature within the ice pack [*Comiso*, 1983; *Parkinson et al.*, 1987]. The advent of multichannel systems, such as the SMMR, allowed the development of algorithms that circumvent this problem [*Cavalieri et al.*, 1984; *Svendsen et al.*, 1983; *Swift et al.*, 1985; *Comiso*, 1986]. Such algorithms have been further refined to take advantage of the added capabilities of the AMSR-E sensor [*Markus and Cavalieri*, 2000; *Comiso et al.*, 2003]. This study makes use of the bootstrap algorithm that utilizes the 19- and 37-GHz channels at vertical polarization and the 37-GHz channel at horizontal polarization for both hemispheres, as described in *Comiso* [2004]. The 89-GHz data have been used in ice retrieval algorithms as well but sensitivity to atmospheric and snow cover effects is high and a radiative transfer program [*Kumerow*, 1993] to correct these effects is needed.

[8] The satellite era started with the Nimbus-5/Electrically Scanning Microwave Radiometer (ESMR) which was launched in December 1972 and was the first microwave imaging (or scanning) system. The ESMR provided some useful sea ice data during the 1973 to 1976 period but it is a one-channel system and there are many data gaps (sometimes several months in a year) because of hardware related problems. Trend studies of the sea ice cover usually make use of SMMR and SSM/I data which provide continuous coverage from November 1978 to the present. Even with this restriction, assembling a data set using SMMR and SSM/I is not trivial because of different attributes and characteristics of each sensor. The advent of AMSR-E data starting in June 2002 represents a considerable improvement in capability, but combining these data with SMMR and SSM/I data is again a big challenge. Mismatches in the locations of the ice edges can occur because of different resolutions, antenna patterns (i.e., side lobes) and other factors including different times of visit in ice covered regions where divergent ice floes and decaying or flooded ice are prevalent. The slight differences in peak frequencies, incident angles and calibration can also make a difference.

[9] The AMSR-E has become the passive microwave instrument of choice because of higher resolution, greater spectral range and wider swath and therefore improvements in accuracy and coverage. The higher resolution alone enables estimates of more accurate ice concentrations from AMSR-E than from other passive microwave sensors because within the smaller satellite footprints, there are less number of different surface types and therefore less ambiguity in discriminating open water from sea ice, using equation (1). It also enables improved representation of ice edges and ice features. AMSR-E brightness temperature [T_B(AMSR-E)] data and ice concentrations derived from these T_B data are therefore used as the standard in this study. Consistency between the different satellite data sets was achieved by making data from the other sensors as close to those of AMSR-E as possible. In particular, the T_B data from SSM/I were normalized for each set of channels using parameters derived from linear regression of data from the two sensors during the period of overlap. More specifically, a conversion of the form

$$T_B(\text{SSM/I}) = a + bT_B(\text{AMSR-E}) \quad (2)$$

was applied, where a and b are the fit parameters corresponding to the offset and slope of the regression line, respectively. The T_Bs of SSM/I and AMSR-E are highly correlated with the correlation coefficients being 0.990, 0.983 and 0.980 at 37 GHz(V), 37 GHz(H) and 19 GHz(V), respectively. Similarly, normalization of data sets was performed on SMMR, using the modified SSM/I data as the standard. The T_Bs of SMMR and SSM/I are also highly correlated with the correlation coefficients being 0.960, 0.953 and 0.925 at 37 GHz(V), 37 GHz(H) and 19 GHz(V), respectively. Finally, the same sea ice concentration algorithm (i.e., bootstrap algorithm) as described by *Comiso* [2004] was used to process the data from all sensors and generate the enhanced sea ice data set used in this study. Although it is the same formulation, the bootstrap algorithm will be called ABA when applied to AMSR-E data and SBA when applied to SSM/I and SMMR data.

[10] Examples of enhanced daily ice concentration maps from AMSR-E and SSM/I during the winter periods in the two hemispheres are presented in Figure 2 (i.e., 15 February 2003 in the Northern Hemisphere and on 15 September 2003 in the Southern Hemisphere). In general, the technique works very well with the resulting daily ice concentration maps from the two sensors showing reasonably good agreement during overlapping periods. The difference maps presented in Figures 2c and 2f provide more quantitative comparisons and it is apparent that the same features of the ice cover are captured by the two sensors. There are, however, subtle differences especially near the ice margins where differences as large as ±5% are apparent.

[11] In addition to resolution, other factors can cause different characterization of the ice edge by different sensors. Among these is the way weather effects are taken into account, especially with the slight difference in peak frequencies. In particular, although the midfrequency channel in both sensors is approximately close to 19 GHz, AMSR-E has an 18.7-GHz channel which is farther away from the water vapor line (approximately 22 GHz) than the SSM/I 19.35-GHz channel. The large contrast of the passive microwave signature of sea ice and open water at some of the channels has enabled estimates of reasonably accurate ice concentration except when the signatures of open water

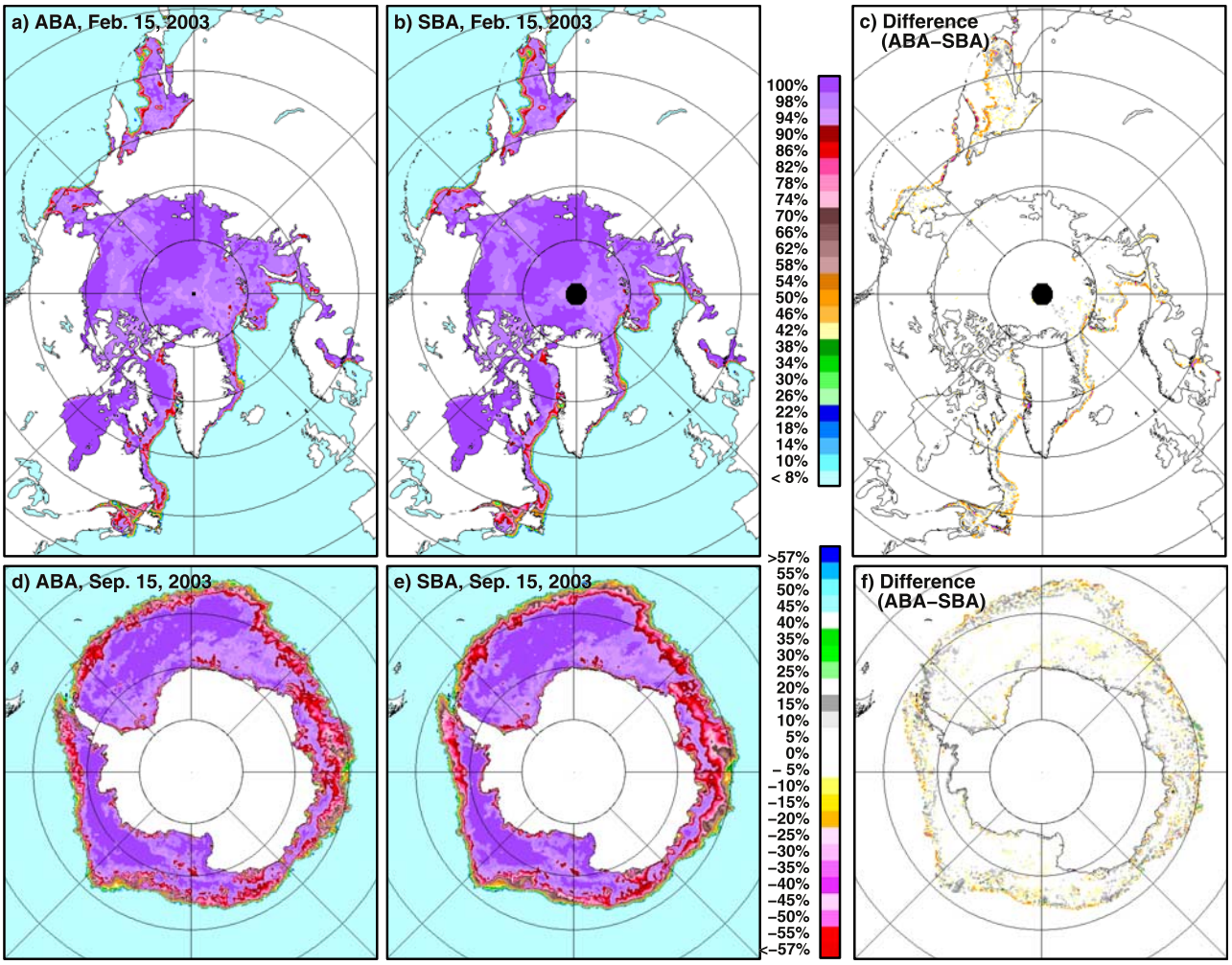

Figure 2. Daily ice concentration maps during winter in the (a) Northern Hemisphere using AMSR-E data, (b) Northern Hemisphere using SSM/I data, (c) difference map between Figures 2a and 2b, (d) Southern Hemisphere using AMSR-E data, (e) Southern Hemisphere using SSM/I data, and (f) difference map between Figures 2d and 2e.

and ice covered surfaces are virtually identical. In particular, areas in the open ocean that are under the influence of inclement weather conditions can have signatures similar to those of ice covered ocean. We make use of a combination of 19-, 22-, and 37-GHz brightness temperatures (T_B) at vertical (V) and horizontal (H) polarizations to discriminate open ocean data from ice data even under unusual conditions. Figures 3a and 3b show scatterplots of $T_B(19,V)$ versus the difference $T_B(22,V)-T_B(19,V)$ using SSM/I and AMSR data, respectively, while Figures 3c and 3d, show the corresponding plots of $T_B(19,V)$ versus $T_B(37,V)$. The gray data points in the scatterplot along a line OW represent data from the open ocean at all weather conditions while the black data points are those from ice covered ocean. In the open ocean the surface gets disrupted occasionally by strong winds and inclement weather causing large surface waves and foam. The microwave signature of open water is thus variable and moves from low values at O to higher values and toward W in the scatterplot, depending on the strength of the disruption. In the algorithm, these data points in gray and are masked to represent open water. Open water brightness temperature data within the ice pack and used

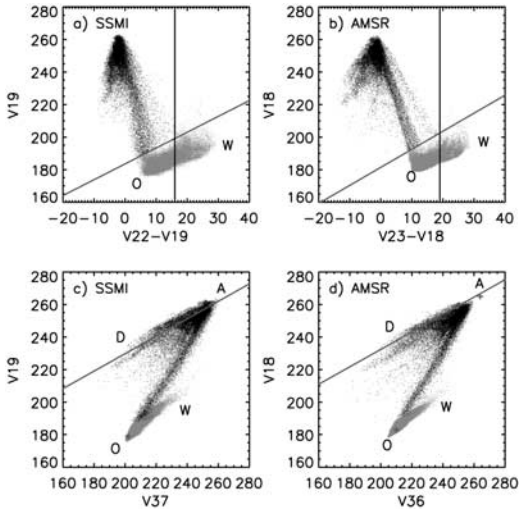

Figure 3. Scatterplots of T_B(V19, V) versus T_B(22, V)-T_B(19, V) for (a) SSM/I and (b) AMSR-E data. Also, scatterplots of $T_B(19,V)$ versus $T_B(37,V)$ for (c) SSM/I and (d) AMSR-E data.

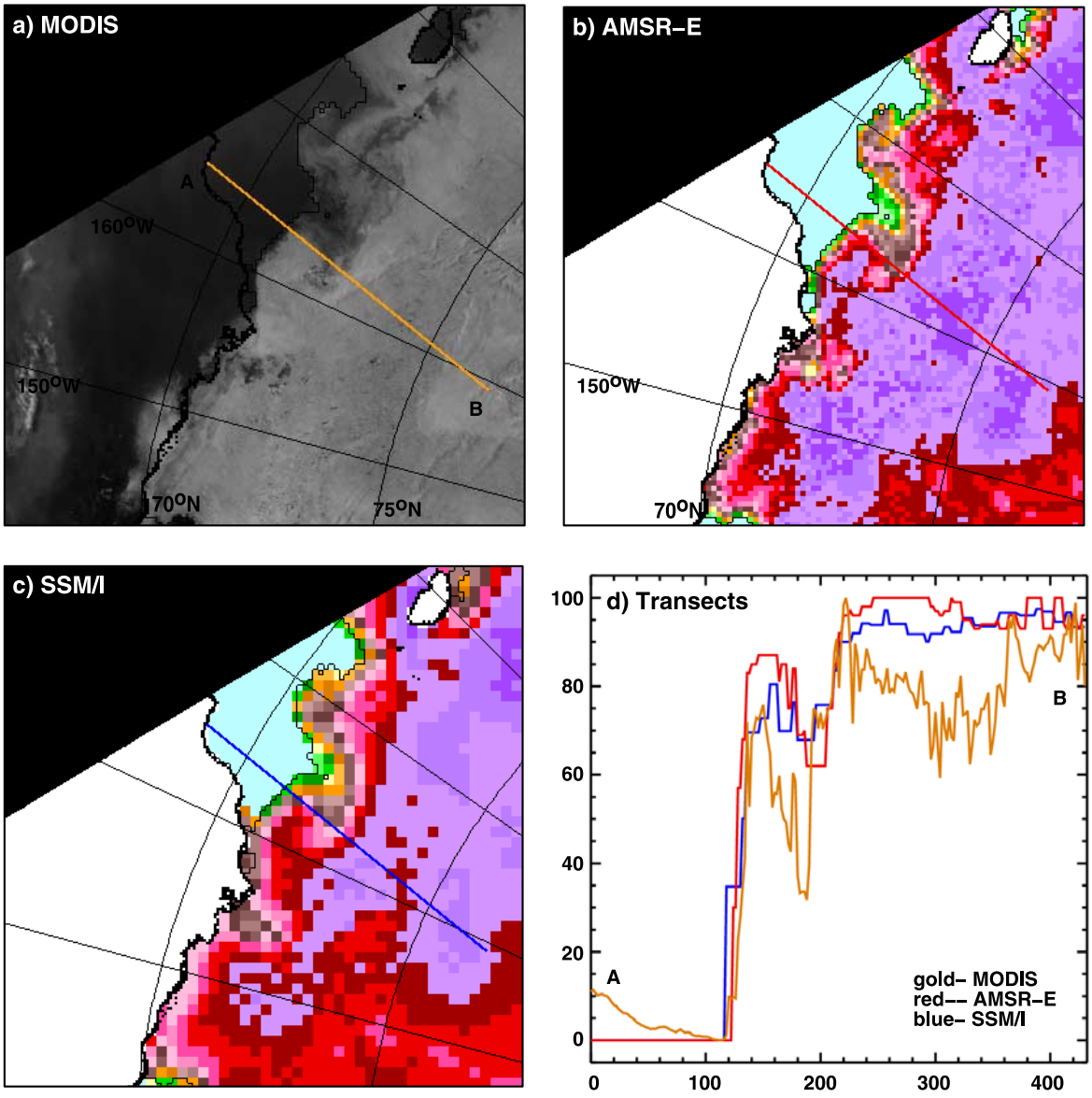

Figure 4. Images of the Beaufort/Chukchi Seas Ice cover in the Northern Hemisphere as depicted by (a) MODIS radiance, (b) AMSR-E ice concentration, and (c) SSM/I ice concentration data. (d) Distribution of radiances from MODIS 0.6-μm channel, AMSR-E ice concentration, and SSM/I ice concentrations along the line transect marked A to B (in the MODIS).

to represent T_O in equation (1) are the low values close to the label O (along OW). The gray line represents approximately 10% ice concentration used as the threshold between ice and open ocean as described by *Comiso et al.* [2003]. Because of significant variability of the emissivity of sea ice near the ice edge, the error in the retrievals near 10% ice concentration is relatively large. We therefore use 15% ice concentration and higher as was done by *Zwally et al.* [1983], instead of 10% and higher, to minimize errors in the estimate of ice extent.

[12] The higher resolution AMSR-E data provide a more defined marginal ice zone than SSM/I data but it is not clear from Figure 2, how the two sensors differ in their assessment of the ice edge location. A comparison of passive microwave measurements with ship observations, have also indicated significant discrepancies in the location of the ice edge, especially during the summer melt period [*Worby and Comiso*, 2004]. Ship observations are valuable but more studies are needed since mismatches between a point measurement from a ship and observations from a much larger area by a satellite sensor can cause misleading information. To gain insight into the accuracy of ice edge locations as observed by satellites, two sets of images that include MODIS data and a plot along a transect that goes across the ice edge are presented in Figures 4 and 5. During clear skies conditions, MODIS data at 0.6 μm with a spatial resolution of 250 m provide a good representation of the sea ice cover and the location of the ice edge because of the large contrast in the albedo of sea ice and open water [*Allison et al.*, 1993]. Images of the Beaufort/Chukchi Seas region during melt conditions on 29 June 2004, as observed by MODIS, AMSR-E and SSM/I, are shown in Figures 4a,

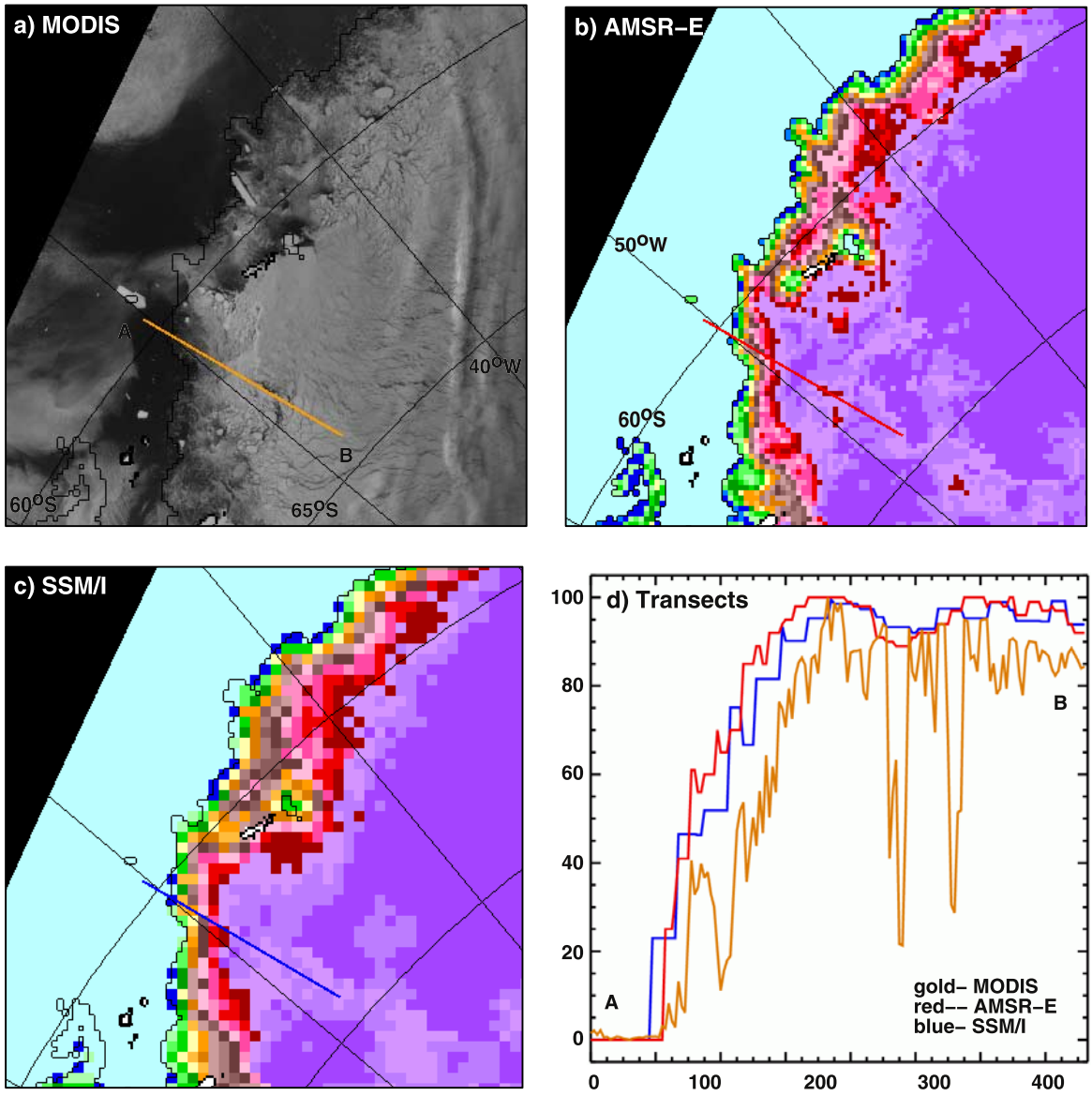

Figure 5. Images of the Weddell Sea Ice cover as depicted by (a) MODIS radiance, (b) AMSR-E ice concentration, and (c) SSM/I ice concentration data. (d) Distribution of radiances from MODIS 0.6-μm channel, AMSR-E ice concentration, and SSM/I ice concentrations along the transect marked A and B (in the MODIS).

4b and 4c, respectively. The MODIS data show detailed characterization of the sea ice cover and mesoscale features both near the ice edges and the inner pack. Comparing this image with the passive microwave images, it is apparent that AMSR-E provides better representation of many of the features of the ice cover observed by MODIS than SSM/I. This demonstrates that higher resolution makes a difference, especially in identifying ice edges, leads, polynyas and other characteristics of the sea ice cover. For a more quantitative comparison, the values from the three images along a transect defined by a line from A to B (see MODIS image) are presented in Figure 4d. The MODIS radiances (in gold), are shown to be relatively low in the open water area (at A) and actually goes down toward the ice edge and then increase substantially to much higher values within the pack. Some fluctuations within the pack are apparent likely owing to the variability of the albedo of sea ice surfaces during this time on account of ice melt, meltponding, ice breakup and decay. The corresponding plots for ice concentrations from AMSR-E and SSM/I are shown by the red and blue lines, respectively. It is apparent that the ice edge location (i.e., where the ice concentrations increases rapidly) as detected by AMSR-E is closer to that identified by MODIS than the SSM/I data. The 15% ice edge detected by the SSM/I is farther south than that detected by AMSR-E by about 12.5 km while the AMSR-E is farther south of MODIS value by less than 6 km. Although the interpretation of MODIS data at the ice edge is complicated by the presence of many new ice types that have different albedos, the location of the ice edge is discernible and appears to be in general agreement with those from passive microwave data.

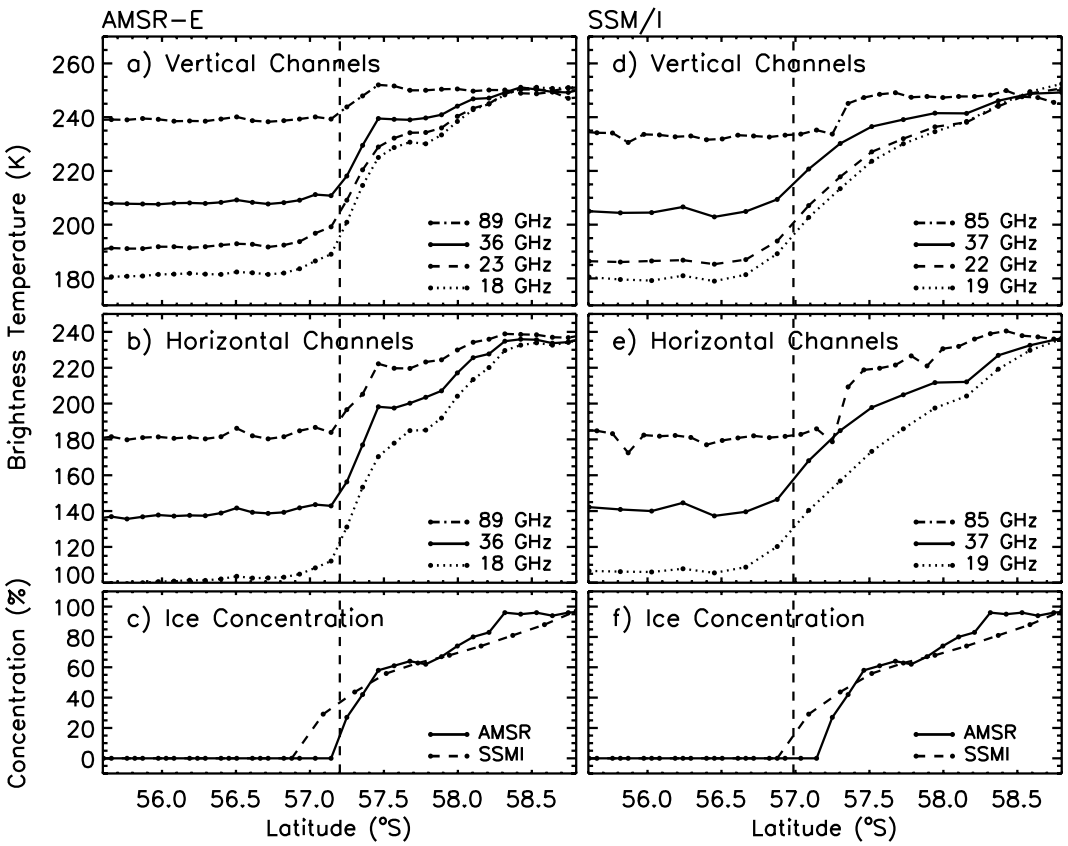

Figure 6. Plots of AMSR-E and SSM/I brightness temperatures along the 0° longitude in the Weddell Sea in the Southern Hemisphere using AMSR-E data at (a) vertical and (b) horizontal polarizations and SSM/I data at (d) vertical and (e) horizontal polarizations. Plots of ice concentrations from AMSR-E and SSM/I data are also shown with the ice edge as determined by AMSR-E and SSM/I indicated by vertical lines in Figures 6c and 6f, respectively.

[13] The set of images presented in Figure 5 is similar to those of Figure 4 but located in the Antarctic and taken on 9 September 2002 when the ice surface is still relatively cold and dry. Again, the spatial distribution of the ice cover as observed in the MODIS image is better reproduced by the AMSR-E image than the SSM/I image both at the ice edge and within the pack. Plots along a transect (labeled A to B) across the ice edge are also presented (Figure 5d). The radiances from MODIS data along this transect show open water signature outside the ice pack as in Figure 4 but at the ice edge, the signature is not so well defined. It increases slightly indicating a wide band of new pancake ice then increases to a maximum value and fluctuate in value within the ice pack. The corresponding transects from AMSR-E and SSM/I show more well-defined ice edges with the SSM/I ice concentrations (blue line) showing an ice edge location that is farther north than the AMSR-E data (red line) by about 10 km. The ice edge location identified by AMSR-E also appears to be closer to that identified by the MODIS image than that identified by SSM/I. In the MODIS image, there are two strong dips within the ice pack region which are not identified as reduced concentrations in the AMSR-E and SSM/I transects. The dips likely represent leads that have been refrozen and have not acquired a snow cover (and hence the relatively low radiances).

[14] To illustrate the effect of resolution on the characterization of the ice edge, plots of AMSR-E and SSM/I brightness temperature data using different frequencies and polarizations are presented in Figure 6. The plots are along a transect in the Weddell Seas at 0° longitude on 21 June 2002 and it is apparent that AMSR-E brightness temperatures at all frequencies and polarizations increases concurrently at the ice edge (Figures 6a and 6b). On the other hand, SSM/I brightness temperatures are less consistent at the ice edge with the 19 GHz channels showing increases (or sensitivity to the ice edge) farther away from the pack than the other channels (Figures 6d and 6e). The effect of the aforementioned coarser resolution of SSM/I channels than AMSR-E channels is evident with the ice edge as identified by the SSM/I 85-GHz channels being farther south (into the pack) and more consistent with those of AMSR-E data. Thus the highest resolution channel from SSM/I is consistent with the AMSR-E data in identifying the ice edge while the other channels show the effect of coarser resolution. Corresponding ice concentration values using AMSR-E and SSM/I data are plotted in Figures 6c and 6f with the vertical lines in the left column representing the ice edge as identified by AMSR-E while those in the right column representing the ice edge as detected by SSM/I. This particular transect shows a difference in ice edge location of about 12 km but such difference can vary

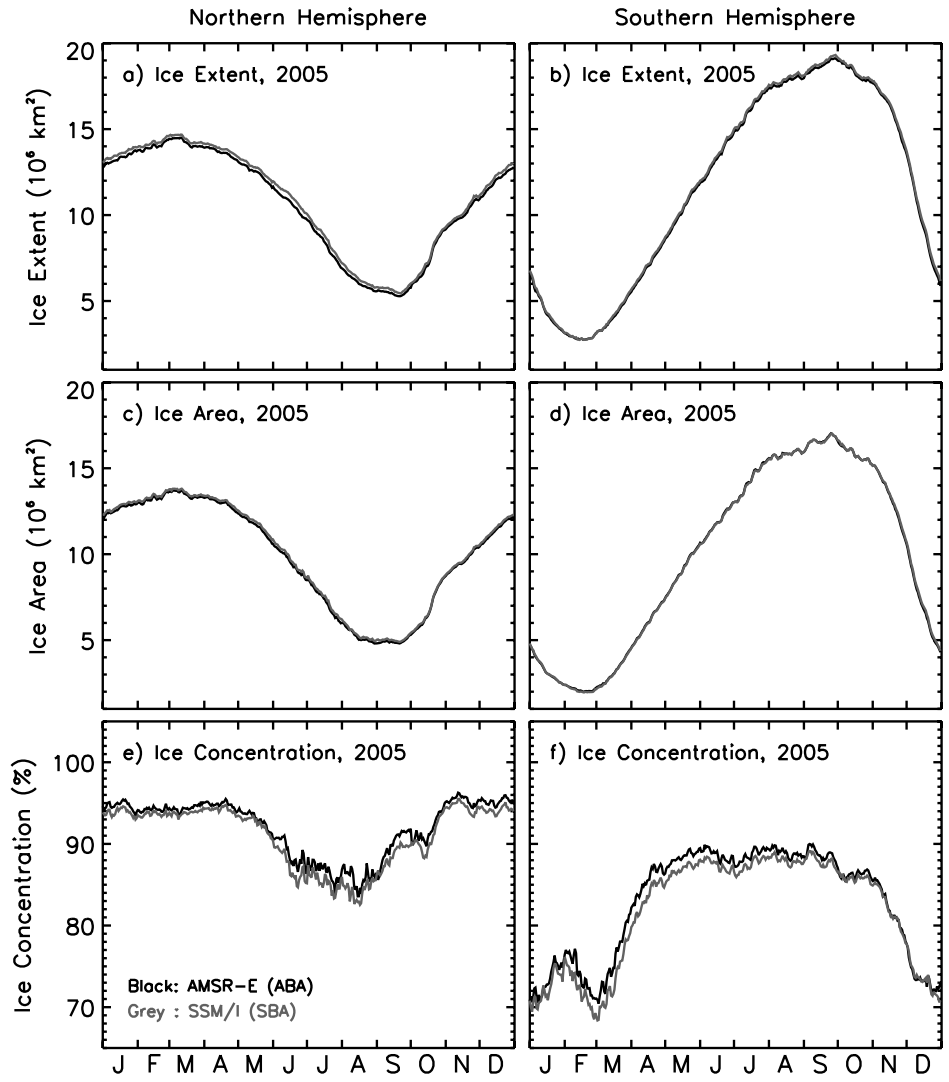

Figure 7. Daily (a, b) ice extents, (c, d) ice area, and (e, f) ice concentration during a period of SSM/I and AMSR-E overlap in 2005 in the Northern and Southern Hemispheres.

from one location to another depending on environmental conditions.

3. Comparison of Sea Ice Extents, Area, and Ice Concentration During Overlap Period

[15] The ice parameters derived from satellite ice concentration data that are most relevant to climate change studies are sea ice extent and ice area. Ice extent is defined here as the integrated sum of the areas of data elements (pixels) with at least 15% ice concentration while ice area is the integrated sum of the products of the area of each pixel and the corresponding ice concentration. Ice extent provides information about how far south (or north) the ice extends in winter and how far north (or south) it retreats toward the continent in the summer while the ice area provides the total area actually covered by sea ice which is useful for estimating the total volume and therefore mass, given the average ice thickness. Quantitative comparisons of AMSR-E and SSM/I data show excellent agreement during overlap period, with the correlation coefficients being 0.9997, 0.9999, and 0.9910 for ice extent, ice area and ice concentration, respectively, in the Northern Hemisphere and almost identical correlation values in the Southern Hemisphere. There are, however, some minor discrepancies that can lead to biases, especially in trend analysis. Figures 7a–7f show distributions of daily average ice extent, ice area and ice concentration over an entire annual cycle using AMSR-E and SSM/I data in 2005 for both hemispheres. The plots in Figures 7a and 7b are for ice extents in the Northern Hemisphere and indicate that the values derived from SSM/I data (in grey) are consistently higher (~1.3%) than those from AMSR-E data (in black) with the difference in winter relatively smaller than in the summer period. A similar set of plots but for ice areas (Figures 7c and 7d) shows better consistency with the SSM/I values only slightly higher (~0.9%) than those derived from AMSR-E data. The higher difference in ice extent than in ice area is a manifestation of the effect of the coarser resolution of SSM/I that leads to a smearing effect at the ice edge as demonstrated earlier and hence to more pixels with ice cover (and hence higher extent) than AMSR-E data. The average ice concentrations from (Figures 7e and 7f) are

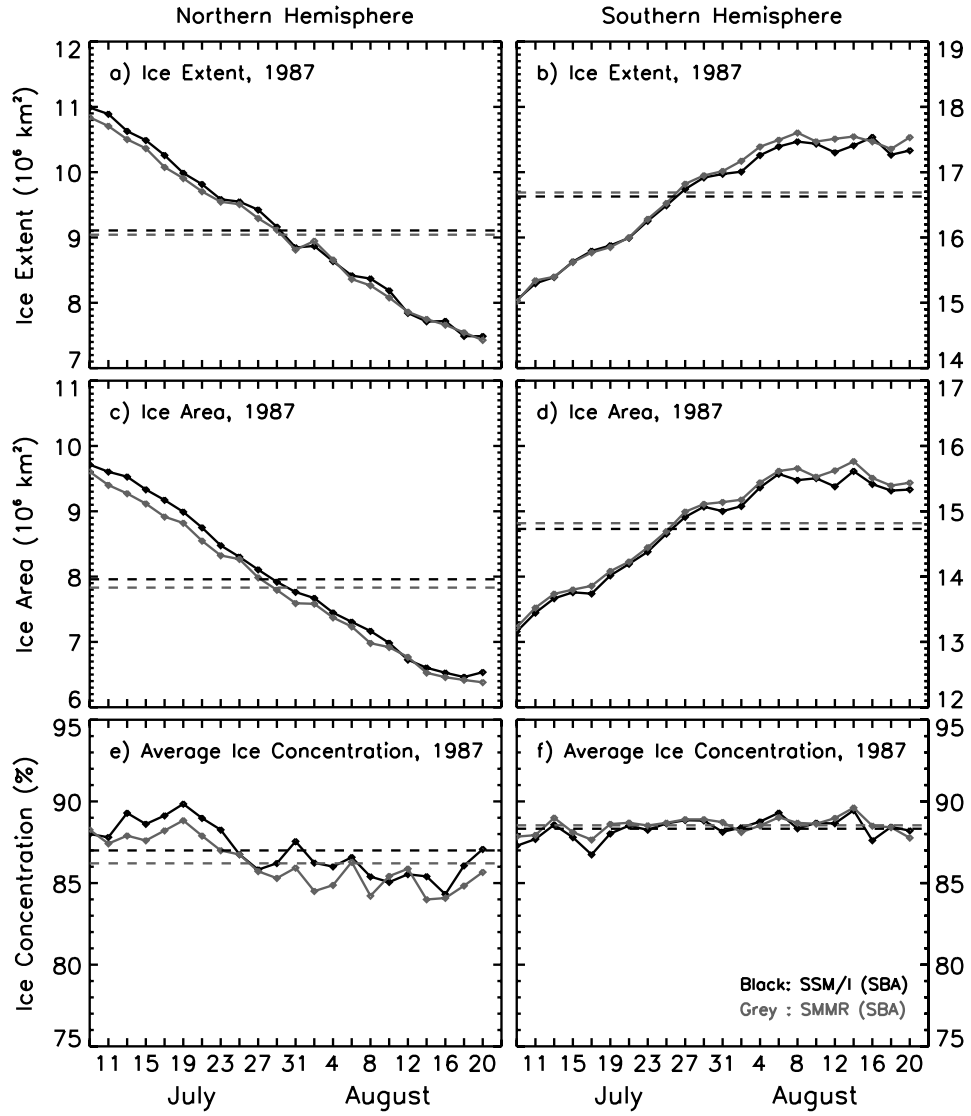

Figure 8. Daily (a, b) extent, (c, d) ice area, and (e, f) ice concentration during a period of SMMR (in grey) and SSM/I (in black) overlap in the Northern and Southern Hemispheres (July to August 1987).

also shown to be consistent and the slightly higher values for AMSR-E than SSM/I (of about 1%) are in part due to more low concentration pixels in the latter occurring mainly at the ice edges.

[16] Similar comparative analyses of ice extents, ice area and ice concentration using data from two SSM/I sensors (i.e., F11 and F13) during the overlap period from May to September 1995 were done and the results show almost perfect agreement (not presented). This is not surprising since the two sensors have practically the same attributes. During the overlap period of SSM/I and SMMR data from mid-July to mid-August in 1987, the extents and areas are also in good agreement (Figure 8). The correlation coefficients are again very high at 0.999, 0.998, and 0.908 for ice extent, ice area and ice concentration, respectively, in the Northern Hemisphere. The corresponding values for the Southern Hemisphere are 0.997, 0.998 and 0.819, respectively.

[17] During this summer period in the Arctic and winter period in the Antarctic the average differences are about 1% and −0.5%, respectively. The agreement was better during August than in July in the Northern Hemisphere but the opposite is true in the Southern Hemisphere. Also, the SSM/I values tend to be higher than those of SMMR in the Northern Hemisphere in July while the reverse is true in the Southern Hemisphere in August. Furthermore, the differences in the average ice concentrations are larger in the Northern Hemisphere than in the Southern Hemisphere and in July, SSM/I values are higher than those of SMMR while the opposite is true in July in the Southern Hemisphere. Such inconsistencies and short overlap period make it difficult to establish whether there is a bias or not. In this study, SMMR data were used to generate the monthly average for July 1987 while SSM/I data were used for the August 1987 monthly.

[18] Despite considerable differences in resolution and other sensor characteristics our results show good agreement in ice extents and areas derived from AMSR-E, SSM/I and SMMR. This is consistent with the assumption that ice

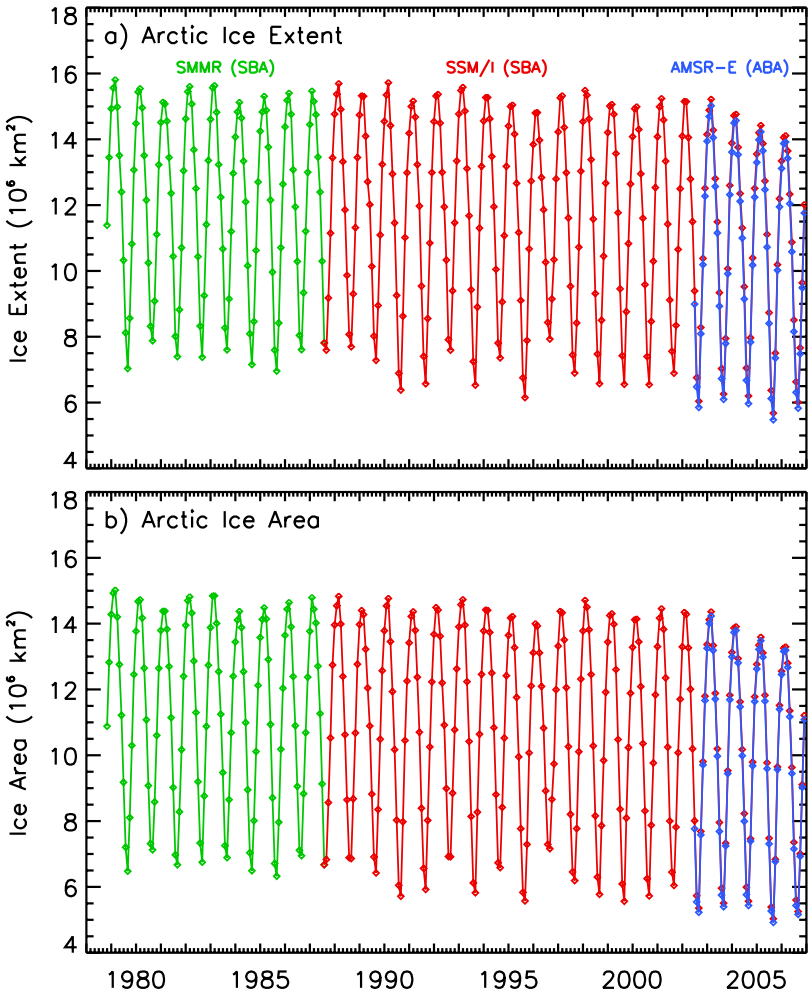

Figure 9. Monthly (a) ice extent and (b) ice area from November 1978 to December 2006 in the Northern Hemisphere using SMMR, SSM/I, and AMSR-E data time series data.

concentration, as defined in equation (1), will generally provide values that are independent of resolution. The biases as quantified are small and the enhanced historical data, including AMSR-E, described in this study are generally consistent and suitable for time series (decadal change) analysis. There are discrepancies, however, especially in ice extent estimates, that can be attributed in part to differences in the antenna side lobes, weather effects and in observation time. The biases can cause significant errors on trend analysis as discussed in the next section.

4. Seasonal Variations and Interannual Trends in Ice Extents and Areas

4.1. Northern Hemisphere

[19] The variability of the sea ice cover in the Northern Hemisphere during the satellite era is summarized by the plots of monthly averages of ice extents and ice areas presented in Figure 9. The temporal variations in the monthly averages are dominated by the large seasonality of the ice cover that fluctuates from minimum values in September to maximum values in February or March. The time series data from SMMR, SSM/I and AMSR are represented in different colors and show a smooth transition from one sensor to the other. For comparison, monthly values from SSM/I and AMSR-E are both presented during the overlap period that started in June 2002 and it is apparent that there is good consistency, especially in ice area.

[20] Figure 9 shows large interannual variability in maximum and minimum values in both extent and area. The patterns are not so predictable with high values in winter not necessarily leading to high values in the summer (e.g., 1979 and 1990) and vice versa. This is a manifestation of the complexity of the Arctic climate system that is driven by both thermodynamic and dynamic factors. It is also apparent that the peak values have been going down since 2002 while the minimum values have been significantly lower than mean values during the same years.

[21] In addition to ice area, the key parameter needed to study the variability of the ice cover is ice thickness. Passive microwave data provide very limited thickness information but they can provide good quantification of the length of thermodynamic growth that is directly related to thickness. The length of growth in our case is defined as the time period from the date of ice minimum in 1 year to the date of ice maximum which occurs the following year. This definition is used because it provides a consistent way to assess

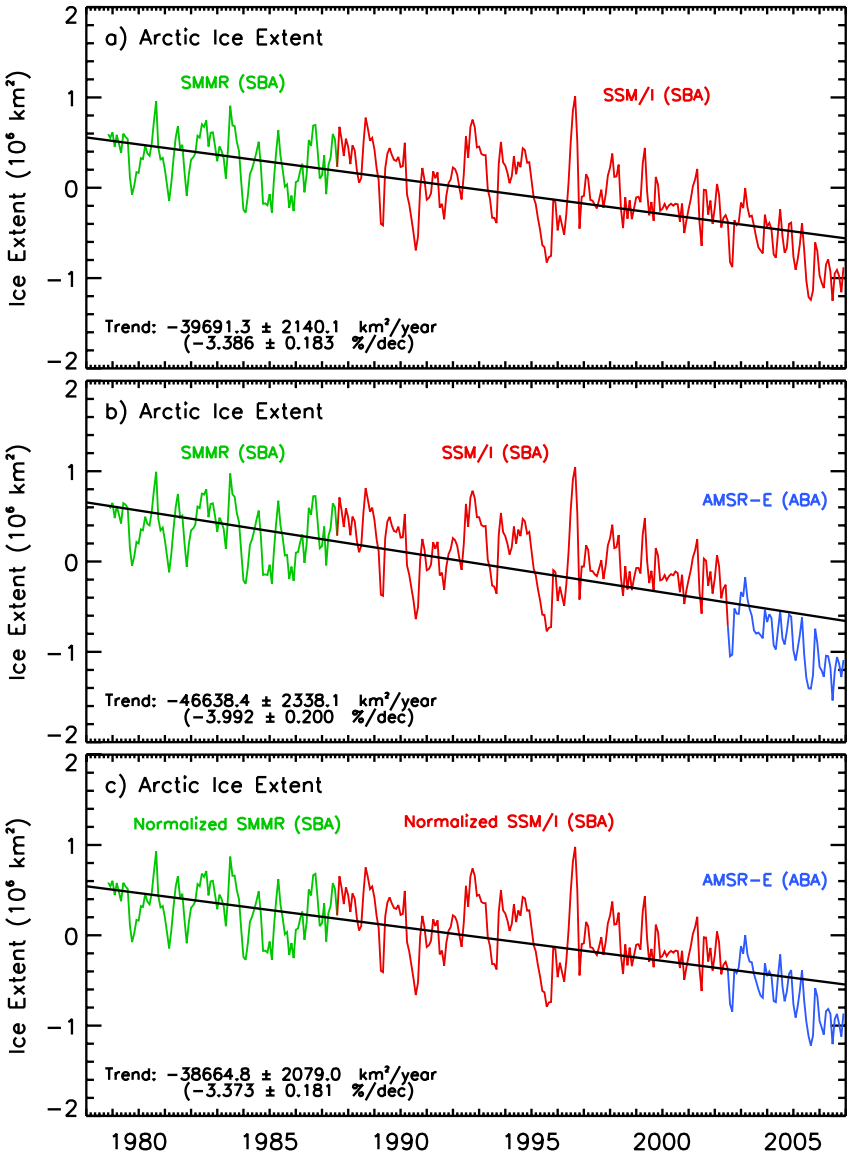

Figure 10. Monthly anomalies and trends in extents from November 1978 to December 2006 in the Northern Hemisphere using (a) original SMMR and SSM/I data; (b) original SMMR, SSM/I (up to May 2002), and AMSR-E data (June 2002 to 2006); and (c) normalized SMMR and SSM/I data and original AMSR-E data.

the length of growth for each year despite the realization that some ice growth actually occurs in parts of the Arctic before the date of ice minimum. Using daily satellite data from 1979 to 2006, the length of growth was found to be declining at a rate of −2.5 days per decade with the average length of ice growth being 179 days. Our analysis also indicated a slight shift in the occurrence of minimum ice extent to a later period with earliest date of minimum occurring on 26 August 1980 and the latest date occurring on 30 September 1995. Such shift in onset of growth suggests a warming ocean which together with the declining length of growth would mean a thinning ice cover.

[22] To assess interannual trends in the ice cover, we use monthly anomalies as has been done previously [*Parkinson et al.*, 1999; *Zwally et al.*, 2002] in order to minimize the effect of the large seasonal variations. These anomalies were obtained by subtracting the monthly climatological averages from each monthly average. The climatology for each month is the average of all data for this month from November 1978 to December 2006. The monthly anomalies for the ice extents in the Northern Hemisphere are presented in Figure 10 in three different combinations, namely: (Figure 10a) SMMR and SSM/I extents only, (Figure 10b) SMMR, SSM/I and AMSR-E extents with SSM/I data ending where AMSR-E data starts, and (Figure 10c) normalized SMMR and SSM/I and original AMSR-E extents. Normalization parameters for the last case are derived from data during SSM/I and AMSR-E overlap and are meant to correct inconsistencies during the period. The first case provides the data that is currently being utilized for trend studies while the second case make use of AMSR-E data instead of SSM/I when the former became available in June 2002. The trend values for SMMR and SSM/I data only is −3.39 ± 0.18% per decade while that for unnormalized

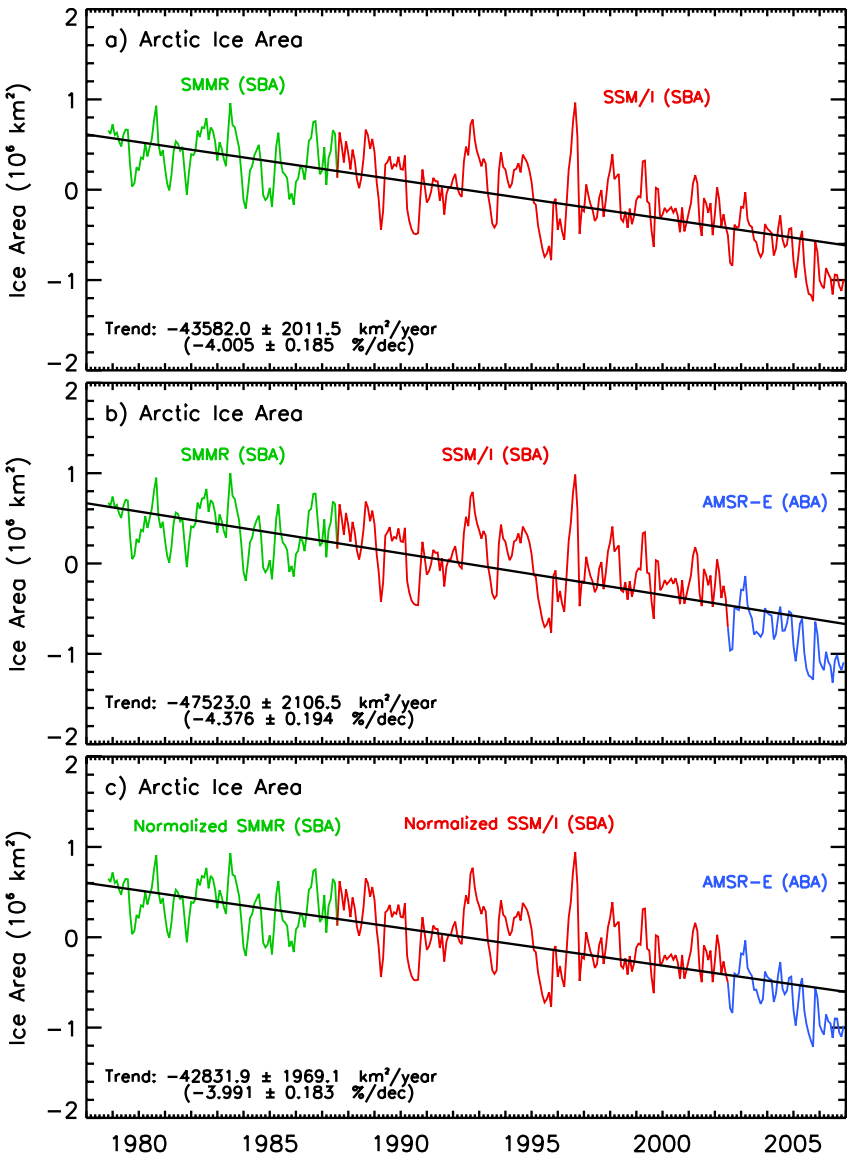

Figure 11. Monthly anomalies and trends in ice area from November 1978 to December 2007 in the Northern Hemisphere using (a) original SMMR and SSM/I data; (b) original SMMR, SSM/I (up to May 2002), and AMSR-E (June 2002 to 2006) data; and (c) normalized SMMR and SSM/I data and original AMSR-E data.

SMMR, SSM/I and AMSR-E data is −3.99 ± 0.20% per decade. There is a difference of −0.60% per decade in the trends but this is likely associated with the bias as described earlier, owing in part to the difference in resolution between AMSR-E and SSM/I. When the bias is removed through aforementioned renormalization, the trend for a combined SMMR, SSM/I and AMSR-E data is −3.37% per decade, which is consistent with that when only SSM/I and SMMR data are used. Since the accuracy of AMSR-E is higher than those of the other sensors, the inclusion of AMSR-E is desirable, even if the trend results are basically the same since the resulting errors on the trends would be smaller as discussed in the next section. The importance of the use AMSR-E data in trend studies will increase with time as the record length of this data set increases.

[23] The range of variability in the anomalies is about 1 × 10^6 km^2 while that of the monthly averages is about 8 × 10^6 km^2 associated with the large seasonality of the ice cover. It is also apparent that the variability is significantly less for the period 1996 to 2006 than previous years. This is intriguing since the slope of the data during the latter period appears different from those of the earlier period. Linear regression using only data from 1996 to 2006 yields a negative trend of more than −8% per decade, which is about twice the trend from 1978 to 2006. During the last 10 years, many unusual events happened in the Arctic. First, a record high ice free region occurred in the Beaufort Sea in 1998 [*Comiso et al.*, 2003] which was then the warmest year on record globally over a century. There was also a record low perennial ice cover in 2002 which was also the warmest year on record at that time. The perennial ice cover was a record low again in 2005 which was the warmest year on record. It is possible that the values before 1996 are representative of the natural variability of sea ice cover in

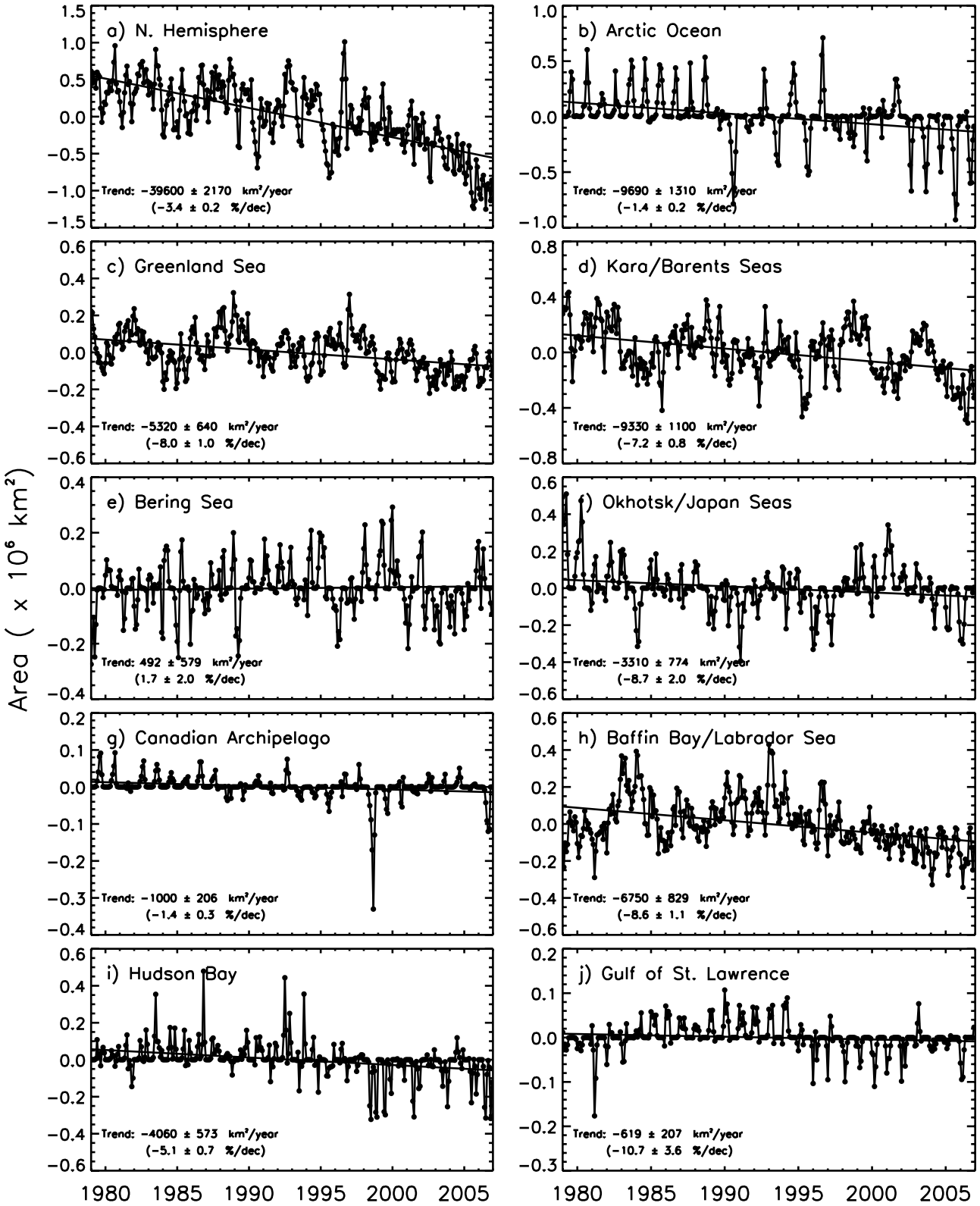

Figure 12. Monthly anomalies of ice extent and trend results in the (a) Northern Hemisphere and in the following regional sectors: (b) Arctic Ocean, (c) Greenland Sea, (d) Kara/Barents Sea, (e) Bering Sea, (f) Okhotsk/Japan Seas, (g) Canadian Archipelago, (h) Baffin Bay/Labrador Sea, (i) Hudson Bay, and (j) Gulf of St. Lawrence.

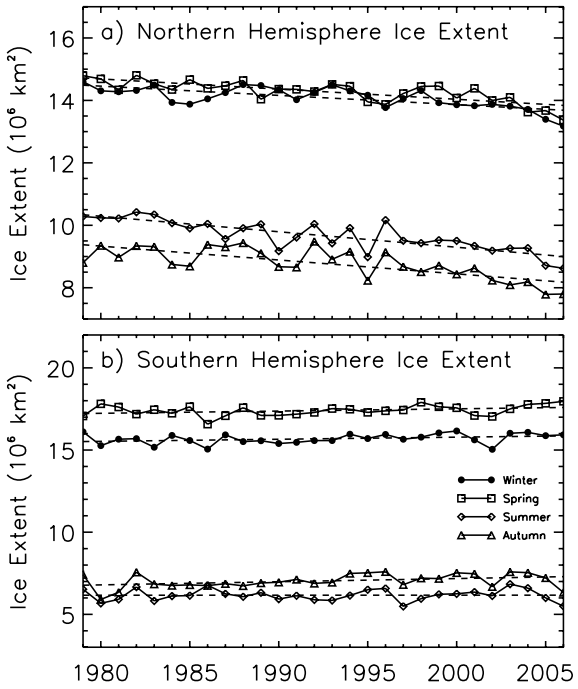

Figure 13. Average ice extents and trends (dash lines) for each season in the (a) Northern Hemisphere and (b) Southern Hemisphere.

the Arctic but those after 1996 may not be part of the natural variability [*Overland*, 2005]. The Arctic ocean surface is expected to warm up as the perennial ice continues to retreat as a result of the ice-albedo feedback, and a warmer ocean would delay the onset of ice growth in the autumn and cause an earlier melt onset, thereby causing a shorter ice season and hence thinner and less extensive ice cover. With additional warming expected from increasing greenhouse gases in the atmosphere the declining trend is expected to continue in the near future.

[24] Similar plots but for the ice area are presented in Figure 11, and it is apparent that the variabilities are similar but the trends are more negative with the corresponding trends for the three cases being -4.01 ± 0.18, -4.38 ± 0.19 and -4.00 ± 0.18%/decade. The more negative trend for ice area compared to those for ice extent is in part associated with a negative trend in the sea ice concentration during the period. Changes in ice concentration may be caused by changes in wind strength and wind patterns that in turn cause changes in the area affected by divergence. In the summer, it can also be caused by changes in the areal extent of meltponding which causes large errors in the estimate of ice concentration [*Comiso and Kwok*, 1996].

[25] Regional variability was also studied to identify locations where most of the changes are occurring, trends in the anomalies in ice extent in various sectors of the Arctic, as described by *Parkinson et al.* [1999], are presented in Figure 12. Overall, the trend for the entire hemisphere is moderate at about -3.4 ± 0.2%/decade but there are regions where significantly higher negative trends than in other regions are apparent. Among these regions are the Greenland Sea, the Kara/Barents Seas, the Okhotsk Sea, Baffin Bay/Labrador Sea, and the Gulf of St. Lawrence where the trends are -8.0, -7.2, -8.7, -8.6, and -10.7%/decade, respectively. In these regions, some cyclical patterns are also evident especially in the first 15 years of data. The only region that show positive trend is the Bering Sea where ice cover appears to be growing but at a negligible rate of 1.7 ± 2.0%/decade. This region is one of the few sea ice covered areas in the Arctic that has exhibited some cooling in the last few decades [*Comiso*, 2006].

[26] For completeness, average ice extents during winter (December, January and February), spring (March, April and May), summer (June, July and August) and autumn (September, October and November) and also trend lines for each season are presented in Figure 13a for the period 1979 to 2005. Significant yearly fluctuations are again apparent, and are especially large and correlated during summer and autumn. The trends are most negative during summer and autumn at -5.13 ± 0.69 and -5.06 ± 0.90%/decade, respectively, and least negative during spring and winter at -2.28 ± 0.38 and -2.10 ± 0.41%/decade, respectively. Changes are thus more pronounced during the summer and autumn than in winter and spring. It should be pointed out that seasonal bias, as observed by *Worby and Comiso* [2004] will not affect the estimate of seasonal trends. Note also that the updated trends of ice extent and area during ice minimum are -8.4 ± 1.4 and -9.6 ± 1.4%/decade, respectively, which are significantly higher that those in summer and autumn.

4.2. Southern Hemisphere

[27] Monthly extents and ice areas in the Southern Hemisphere, as derived from SMMR, SSM/I and AMSR data (Figure 14) show an even more seasonal ice cover than that of the Northern Hemisphere. Minimum ice extents and ice areas usually occurs in February while maximum ice extents and ice areas occurs in September. This means that the growth period takes a longer time than the melt period in the Southern Hemisphere (see also Figure 7). The maximum and minimum extents and areas go though interannual fluctuations but they appear relatively stable. However, it appears that since the winter of 2002, the maximum values have been increasing but at the same time, the minimum values have been decreasing. It would be interesting if the subsequent years would follow the same pattern and show some modulation in the ice cover.

[28] The monthly ice extent anomalies are again presented for the three cases in the Southern Hemisphere (Figure 15) as in the Northern Hemisphere. It is apparent that there was a large fluctuation in the monthly anomalies (of about 2×10^6 km^2) from 1978 through 1987 and then a much more moderate variation (of about 1×10^6 km^2) from 1987 to 1994 that is followed by a larger fluctuation from 1994 through 2006. The monthly extents (Figure 14) do not show large interannual changes during the 1987 to 1994 period and it is not known why the sea ice cover anomalies would go into such transition from high to low variability and then higher variability in the Southern Ocean. Using SMMR and SSM/I data only, the trend in the hemispheric ice extent is 0.945 ± 0.230%/decade while with SMMR, SSM/I, and AMSR-E data, the trend is slightly lower at 0.684 ± 0.230%/decade. The difference is again likely associated with differences in resolution as discussed earlier and if SMMR and SSM/I data are normalized to make them consistent with AMSR-E data, the trend is similar to the

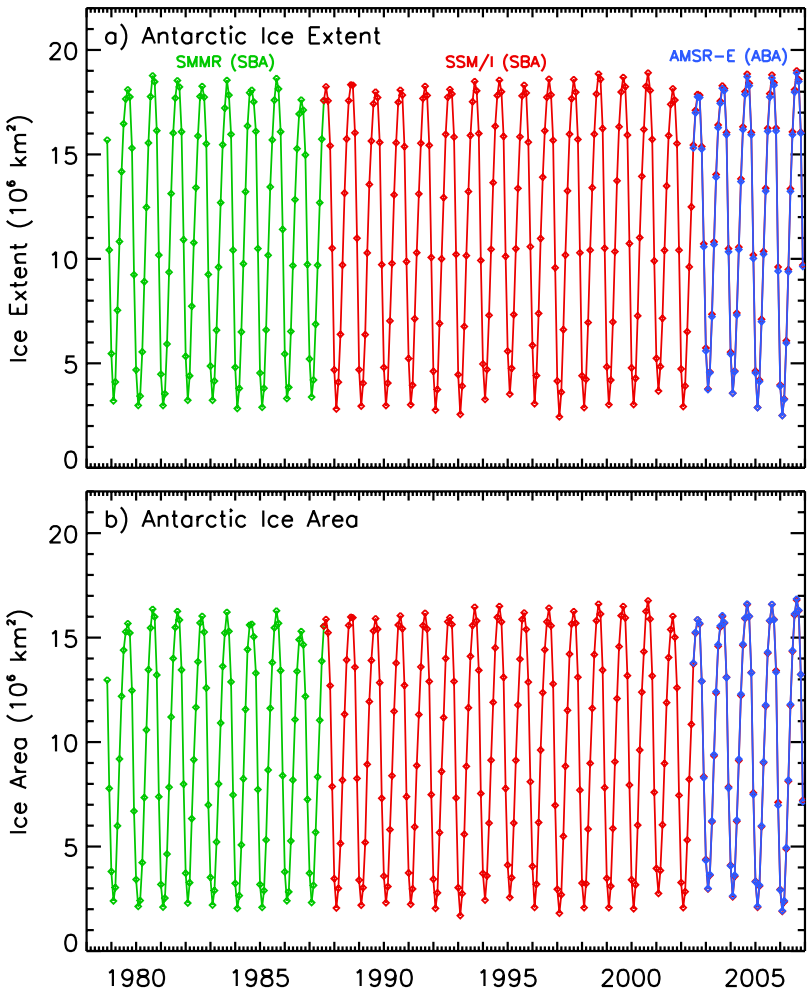

Figure 14. Monthly (a) ice extents and (b) ice areas from November 1978 to December 2006 in the Southern Hemisphere using SMMR SSM/I and AMSR-E data.

first, being 0.94%/decade. In this way, AMSR-E data can be used in conjunction with historical data for decadal change and trend studies.

[29] The corresponding monthly anomalies for ice area as presented in Figure 16 show the same variability as the ice extent. However, the trends are much more similar in the first two cases the values being 1.72 ± 0.25 and 1.77 ± 0.26%/decade. Again, the difference of the first two are minor because the contribution of additional pixels along the ice edge caused by differences in resolution is likely negligible and does not affect the estimate of area as much as that of the ice extent. After the application of the normalization factors on the SMMR and SSM/I data, the trend in as indicated in Figure 16c of 1.72 ± 0.25%/decade is virtually identical to that of Figure 16a.

[30] Except for the summer, the sea ice cover around the Antarctic continent is contiguous and therefore, there is no natural boundary as in the Arctic region. For regional studies, we adapt the same sectors used by *Zwally et al.* [1983]. The monthly anomalies for the entire hemisphere and for the different regions, as presented in Figure 17, have very similar variabilities with the possible exception of those in the Ross Sea Sector. The trends in ice extent for the various regions are all positive except that of the Belingshausen-Amundsen Seas Sector, which has been previously identified by *Jacobs and Comiso* [1997] as a climatologically anomalous region. The trend in this region is currently −5.7%/decade but this is compensated by a positive trend of 4.2%/decade in the Ross Sea. Some declines in the Ross Sea ice cover are apparent in recent years but they are more than compensated by increases at the Indian Ocean and the west Pacific Ocean.

[31] The seasonal trends in the ice extent for the entire Southern Hemisphere are presented in Figure 13b. Significant yearly fluctuations are again apparent, and are correlated mainly during summer and autumn. While also true but not so apparent in the Northern Hemisphere, the sea ice in the Southern Oceans is most extensive during the spring period. As reported previously [e.g., *Zwally et al.*, 2002], the trends are also positive with the updated data set, the values being 0.81 ± 0.44, 0.78 ± 0.41, 0.02 ± 1.37 and 2.73 ± 1.38%/decade, respectively. The trends are most significant during the peak of the ice growth period in autumn.

5. Seasonal Biases and Error Analysis

[32] Comparative studies of ice edges as observed by ship and by satellites by *Worby and Comiso* [2004] indicated

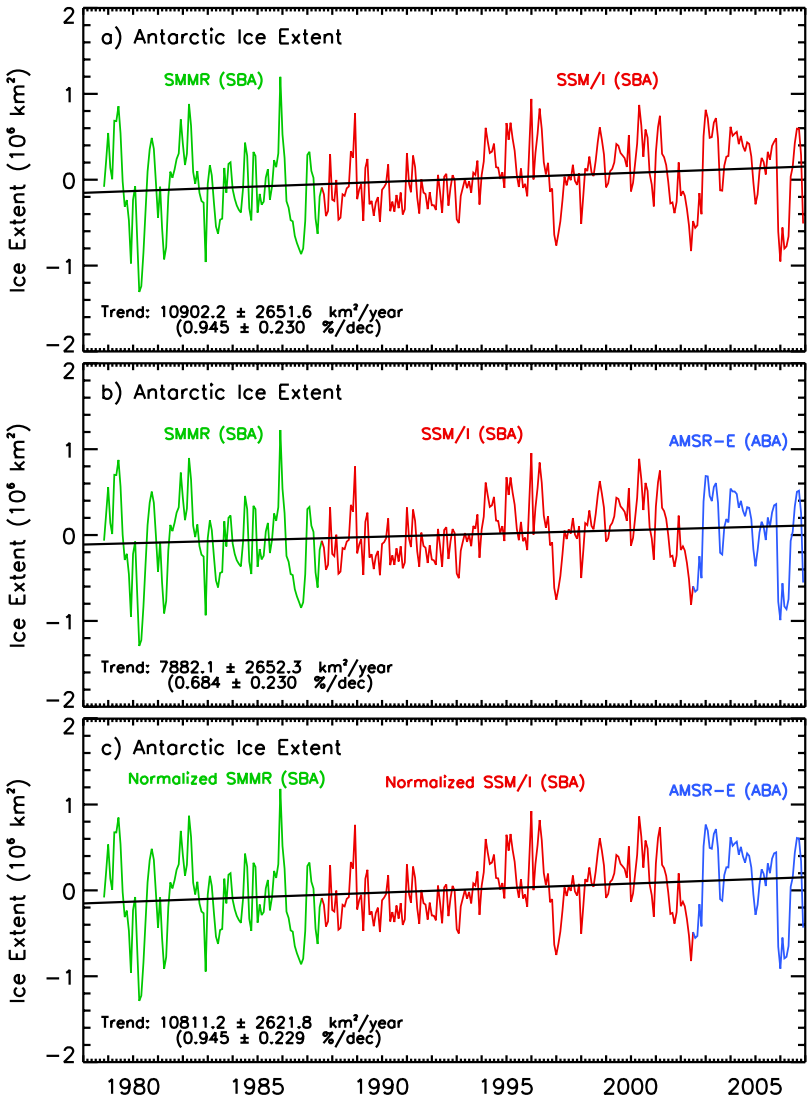

Figure 15. Monthly anomalies and trends in extents from November 1978 to December 2006 in the Southern Hemisphere using (a) original SMMR and SSM/I data, (b) original SMMR, SSM/I (up to May 2002) and AMSR-E (from June 2002 to December 2006), and (c) normalized SMMR and SSM/I data and original AMSR-E data.

significant discrepancies in ice edge location, depending on season. In the summer, they found that the ice edge as determined from ship observations is located farther away from the pack than as observed by satellite data by several kilometers while in the winter, a slight discrepancy in the opposite direction was observed. Trends estimated for the different seasons in the previous section will not to change since applying different biases the for different seasons will not change the slope of the data points in the time series. What could change is the interannual trend when a bias correction is applied consistently during the same season (i.e., June to September in the Arctic and November to February in the Antarctic) from one year to another. As a sensitivity check, we increased the location of the ice edge by 25 km farther away from the pack during the melt periods of each year from 1979 to 2005. The resulting anomalies in extents before and after the application of the 25-km increase in ice edge location for both hemispheres are presented in Figure 18. In the Northern Hemisphere, the trends increased from $-39{,}691 \pm 2140$ km^2/a (-3.4 ± 0.2%/decade) to $-40{,}157 \pm 2158$ km^2/a (-3.3 ± 0.2%/decade) while in the Southern Hemisphere the trends increased from 10,902 km^2/a (0.9 ± 0.2%/decade) to 11,001 km^2/a (0.9 ± 0.2%/decade). A slight but very minor change is apparent from these results suggesting that errors in detecting the ice edge because of changing surface emissivity during the melt period may not affect the trend results significantly. Also, considering the difficulty of matching ship observations with satellite observations, more work needs to be done to establish the magnitude of any associated bias.

[33] To evaluate quantitatively, how differences in sensor characteristics (e.g., resolution) affect the estimates of the trends in ice extent and ice area, we use the original data from SMMR and SSM/I but adjust the location of the ice edge in the AMSR-E data by 25 km farther away from the

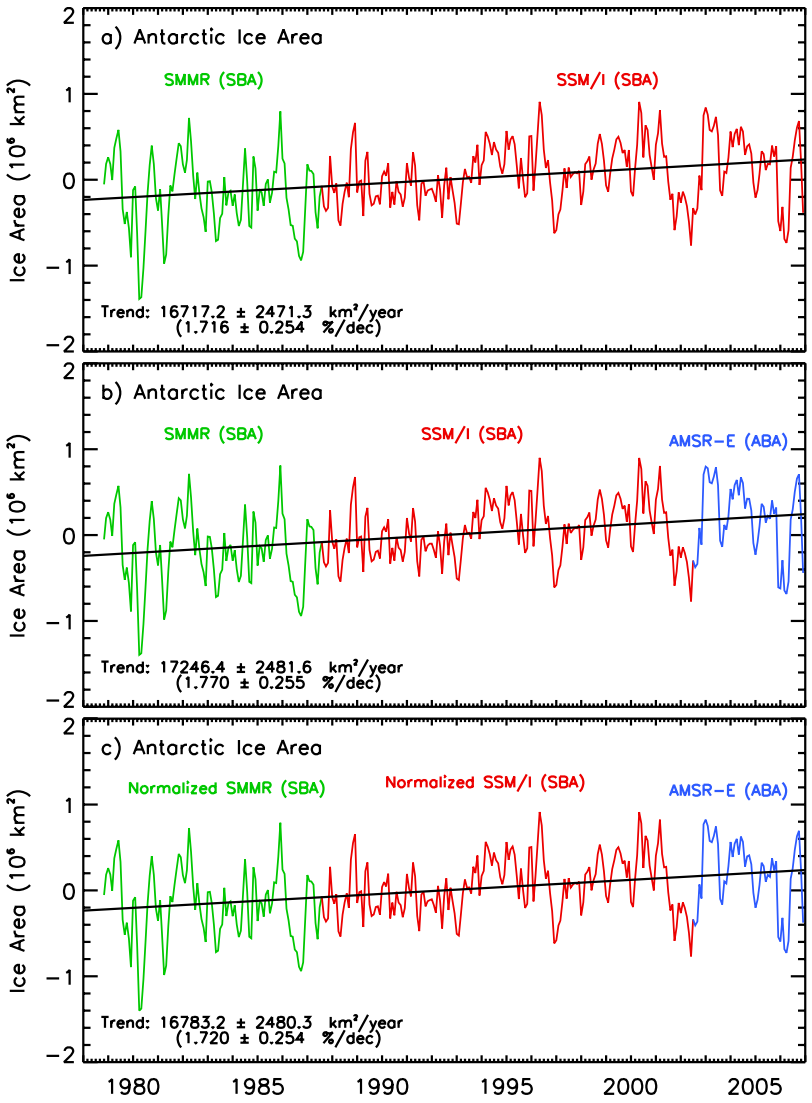

Figure 16. Monthly anomalies and trends in ice area from November 1978 to December 2007 in the Southern Hemisphere using (a) original SMMR and SSM/I data; (b) original SMMR, SSM/I and AMSR-E data; and (c) normalized SMMR and SSM/I data and original AMSR-E data.

ice pack. We also did the same for half a pixel and then a quarter of a pixel to assess the effect of an ice edge being 12.5 and 6.25 km farther away as well. The results are presented in Figures 19 and 20, respectively, for the Northern Hemisphere and the Southern Hemisphere. In the Northern Hemisphere, the trend in extent ranges in value from −3.03%/decade for a 25-km bias in ice edge location of 25-km to −3.99% per decade for no bias. Comparing with our previous results, a bias in the determination of the ice edge or about 14 km would explain the discrepancies observed (i.e., with and without the use of AMSR-E data). In the Southern Hemisphere, the trend in extent ranges from 2.16% per decade for a 25-km bias to 0.68% per decade for no bias. A bias of 6 km in the determination of the ice edge in the Southern Hemisphere would also explain the difference observed.

[34] During the June 2002 to December 2006 overlap period, daily data were also analyzed and the dates of occurrences of minimum and maximum values were approximately the same for both AMSR-E and SSM/I. The percentage difference of maximum ice extents and ice areas between SSM/I and AMSR-E are on the average 1.2% and 0.75%, respectively, in the Northern Hemisphere and 0.87% and −0.216% in the Southern Hemisphere. The percentage difference of minimum ice extents and ice area between SSM/I and AMSR-E are 3.17% and 2.52%, respectively, in the Northern Hemisphere and 0.15% and −1.75% in the Southern Hemisphere.

[35] It should be noted that AMSR-E data also has some limitations. The biggest limitation is the short data record which makes it basically unsuitable for trend analysis unless combined with historical data. There are some gaps in the AMSR-E data set caused by instrumental, telemetry and other reasons and in many cases, SSM/I data provide more complete temporal coverage. There is also still a region around the North Pole that is not covered by AMSR-E and other passive microwave data. Currently, we assume

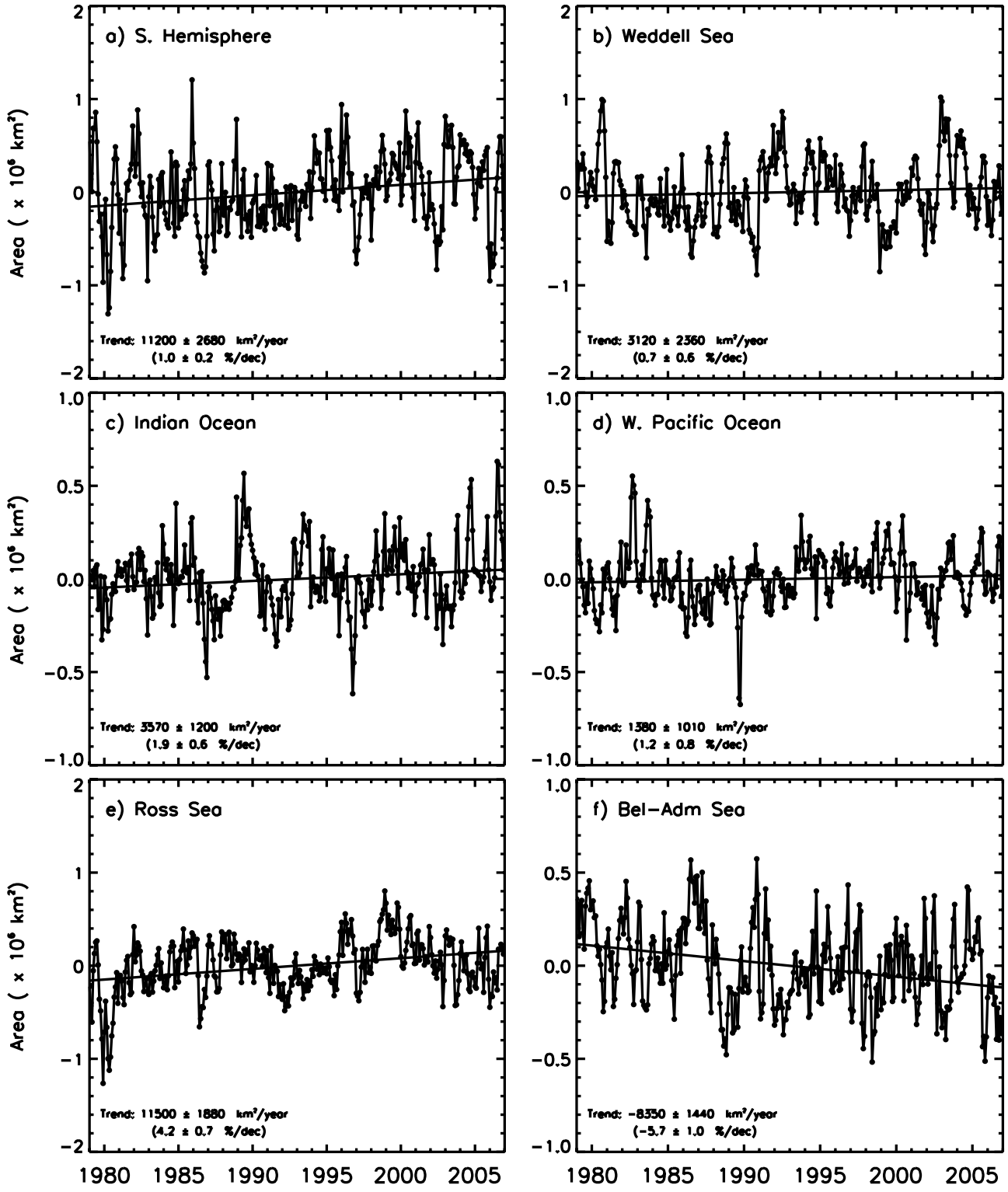

Figure 17. Monthly anomalies of ice extent and trend results in the (a) Southern Hemisphere and in the following regional sectors: (b)Weddell Sea, (c) Indian Ocean, (d) West Pacific Ocean, (e) Ross Sea, and (f) Bellingshausen/Amundsen Seas.

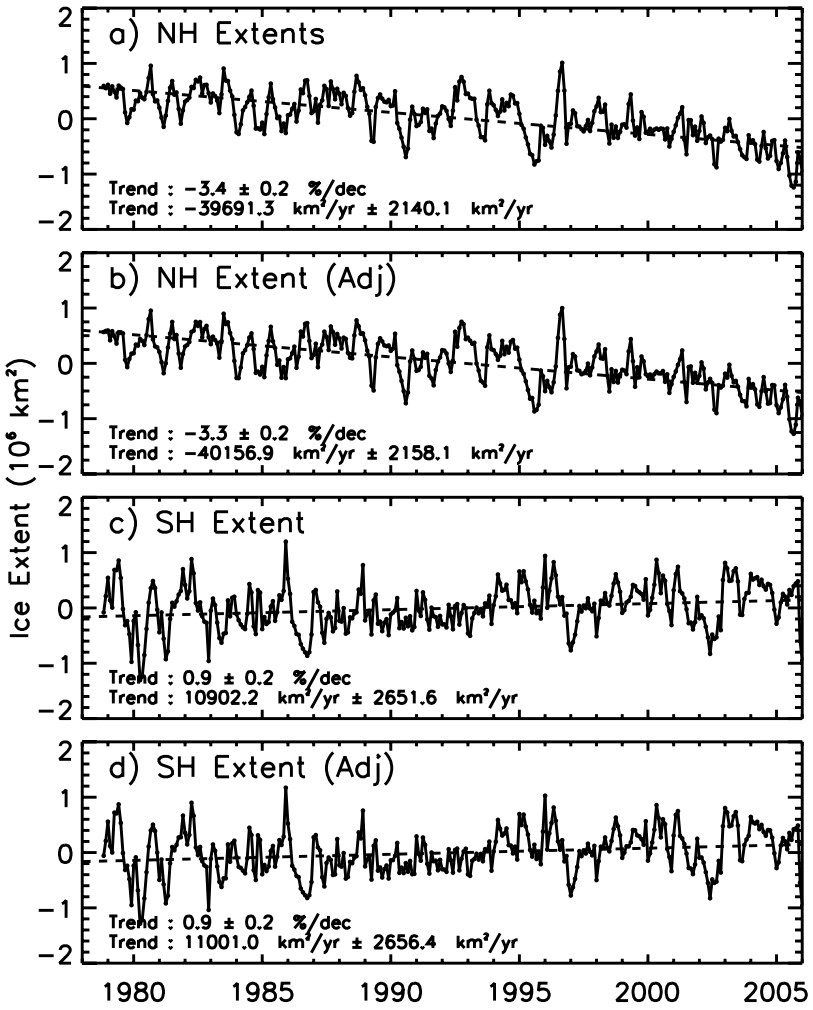

Figure 18. Sensitivity analysis during melt periods. (a) Monthly anomalies in ice extents in the Northern Hemisphere from 1979 to 2005 without any adjustment, (b) monthly anomalies in ice extents in the Northern Hemisphere with the extents during melt periods adjusted farther away from the pack by 25 km, (c) monthly anomalies in ice extents in the Southern Hemisphere from 1979 to 2005 without any adjustment, and (d) monthly anomalies in ice extents in the Southern Hemisphere with the extents during melt periods adjusted farther away from the pack by 25 km.

that the region is covered by sea ice with concentrations constant and similar to those of surrounding regions.

6. Discussion and Conclusions

[36] The launch of AMSR-E provided the opportunity to study the sea ice cover at a higher resolution, wider spectral range, and wider swath than was previously available. Higher resolution data enable the determination of sea ice concentrations at better accuracy because there are fewer surface types within each data element thereby reducing ambiguities in the fraction of open water as determined by the ice algorithms. AMSR-E is used in this study as the standard and basis for creating an enhanced historical sea ice data set that can be used for sea ice variability and trend studies. The historical data includes enhanced SSM/I data which are shown to provide very similar ice concentrations compared with the earlier but enhanced SMMR data and the more recent AMSR-E data during overlap periods. Estimates of ice extents and ice area for all three sensors are also shown to be compatible.

[37] There are subtle differences, however, in the estimates of geophysical parameters, likely associated with differences in physical characteristics of the instruments, that can affect the results of trend analysis using the combined data sets. Because of higher resolution, AMSR-E is able to provide more precise locations of the ice edges and more accurate gradients in these regions than those provided by SSM/I and SMMR. This difference is reflected in the estimates of ice extents with AMSR-E providing slightly lower values on account of higher resolution. To be able to use AMSR-E in combination with historical data, such a bias has to be taken into account. Normalization parameters are inferred to remove the bias using the long period of overlap of AMSR-E and SSM/I data. Sensitivity studies also indicate that the SSM/I ice edge location is about 12 km farther away from the pack in the Northern Hemisphere and about 7 km farther

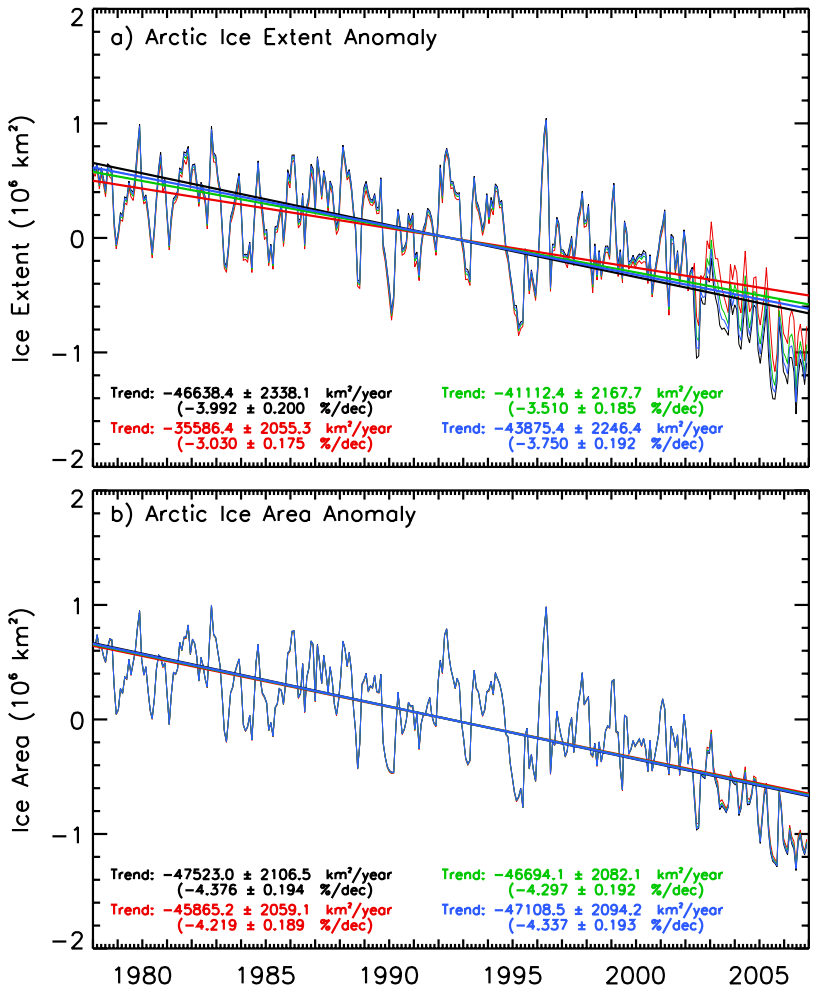

Figure 19. Sensitivity of trends to (a) ice extent and (b) ice area with adjustments of AMSR-E data by making the ice edge 25 km (red), 12.5 km (green), and 6.25 km (blue) farther away from the ice pack in the Northern Hemisphere during an entire ice season.

away from the pack in the Southern Hemisphere than the AMSR-E ice edge. This would translate into about 2% overestimate in extent in the Northern Hemisphere and also 2% overestimate in the extent in the Southern Hemisphere. The AMSR-E values are vulnerable to some errors as well but are likely much lower than those of SSM/I. In a trend analysis that includes edge detection errors described to be sensor (or resolution) dependent, the overall errors in the trend with AMSR-E data included would be less than those with only SMMR and SSM/I data, making the use of the former desirable.

[38] Previous studies comparing locations of ice edges as inferred from ship observations with those from satellite passive microwave data indicated general agreement but with slight biases in the winter period and significantly more during the melt seasons. This was associated with changing emissivity of sea ice during the melt period and could cause additional errors in trend analysis. Such source of error was studied by adding a constant bias to the extent during the melt season for each year from 1979 to 2005. The difference in trends before and after the bias was introduced was found to be negligible both in the Northern and Southern Hemispheres. The seasonal trends were also provided and a bias that depends on season would only alter the offset but not the trend.

[39] The use of AMSR-E data for long-term variability and trend studies is highly desirable especially to ice extent trend studies because the data provide more accurate values than other passive microwave sensors. However, biases in the use of AMSR-E data when combined with SSM/I and SMMR data if uncorrected could also contribute to errors in the estimates of trends in extents of as much as 0.62%/decade in the Arctic and 0.26%/decade in the Antarctic. The biases in ice area are less with the error in the trend of areas being at 0.30%/decade in the Arctic and 0.05%/decade in the Antarctic.

[40] Using data from SMMR, SSM/I and AMSR-E and after correcting for the aforementioned bias, the results of our regression analysis for period from November 1978 to December 2006 yielded trends in extent and area of sea ice in the Arctic region are -3.4 ± 0.2 and -4.0 ± 0.2% per decade, respectively. The corresponding values for the Antarctic region are 0.9 ± 0.2 and 1.7 ± 0.3% per decade. These trend values are comparable to previous estimates

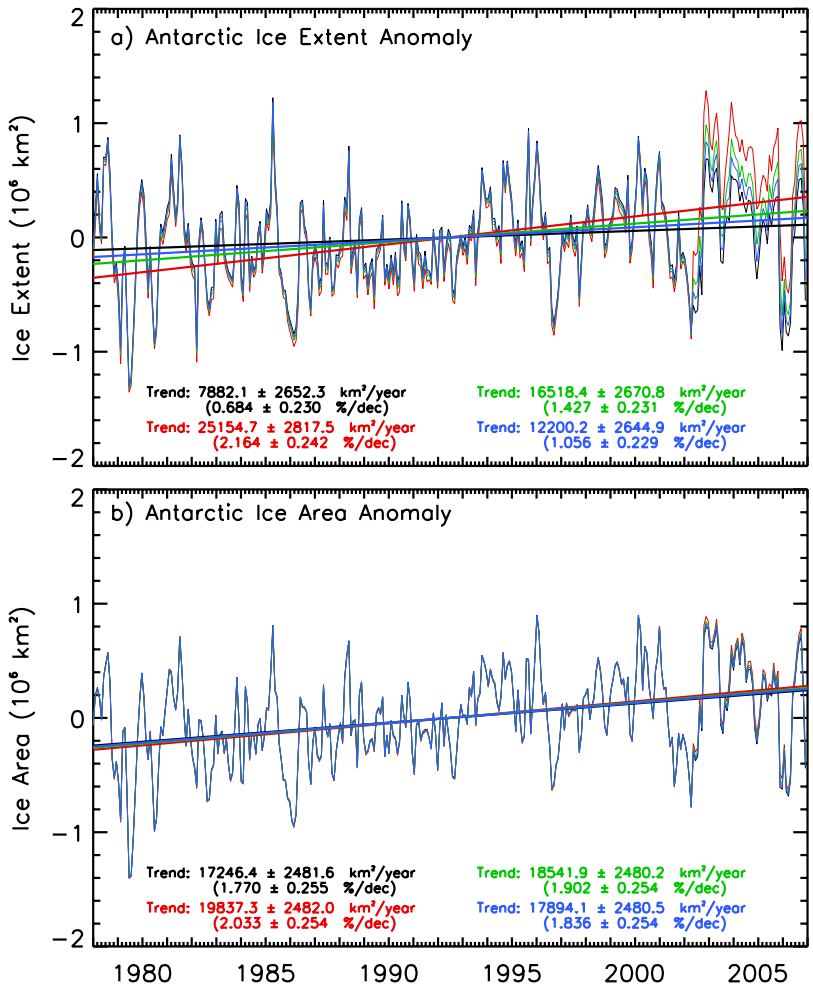

Figure 20. Sensitivity of trends to (a) ice extent and (b) ice area with adjustments of AMSR-E data by making the ice edge 25 km (red), 12.5 km (green), and 6.25 km (blue) farther away from the ice pack in the Southern Hemisphere during an entire ice season.

[e.g., *Parkinson et al.*, 1999; *Zwally et al.*, 2002; *Stroeve et al.*, 2004] and the differences are relatively small despite the longer record and a different processing technique used in this study. Trends in extent in the various sectors of the Arctic are all negatives ranging from −1.4 in the Canadian Archipelago to −11%/decade at the Gulf of St. Lawrence, with the exception of a positive trend of 1.7%/decade in the Bering Sea. Trends in the various sectors of the Antarctic are all positive ranging from 0.7%/decade in the Weddell Sea to 4.2%/decade in the Ross Sea, except at the Bellingshausen/Amundsen Seas sector which is declining at −5.7% per decade. These trends are basically the same as those derived using SMMR and SSM/I data only, but the trend error would be less when AMSR-E data are used because the latter provides more accurate determination of ice extent and ice area. With time, the data from AMSR-E and similar instruments will increase the reliability of the trend values and our ability to forecast the future of the sea ice cover.

[41] **Acknowledgments.** The authors wish to express gratitude to the excellent programming support provided by Robert Gersten of RSIS/Adnet, Inc. This research was supported by the Cryospheric Sciences Program of NASA Headquarters.

References

Allison, I., R. E. Brandt, and S. G. Warren (1993), East Antarctic sea ice: Albedo, thickness distribution, and snow cover, *J. Geophys Res.*, *98*, 12,417–12,429.

Bjorgo, E., O. M. Johannessen, and M. W. Miles (1997), Analysis of merged SSMR SSM/I time series of Arctic and Antarctic sea ice parameters 1978–1995, *Geophys. Res. Lett.*, *24*, 413–416.

Cavalieri, D. J., P. Gloersen, and W. J. Campbell (1984), Determination of sea ice parameters with the Nimbus7 SMMR, *J. Geophys Res.*, *89*, 5355–5369.

Cavalieri, D. J., P. Gloersen, C. Parkinson, J. Comiso, and H. J. Zwally (1997), Observed hemispheric asymmetry in global sea ice changes, *Science*, *278*(7), 1104–1106.

Colony, R., and A. Thorndike (1985), Sea ice motion as a drunkard's walk!, *J. Geophys. Res.*, *90*, 965–974.

Comiso, J. C. (1983), Sea ice microwave emissivities from satellite passive microwave and infrared observations, *J. Geophys. Res.*, *88*, 7686–7704.

Comiso, J. C. (1986), Characteristics of winter sea ice from satellite multispectral microwave observations, *J. Geophys. Rev.*, *91*, 975–994.

Comiso, J. C. (2002), A rapidly declining Arctic perennial ice cover, *Geophys. Res. Lett.*, *29*(20), 1956, doi:10.1029/2002GL015650.

Comiso, J. C. (2004), Sea ice algorithm for AMSR-E, *Riv. Ital. Telerilevamento*, *30–31*, 119–130.

Comiso, J. C. (2006), Arctic warming signals from satellite observations, *Weather*, *61*(3), 70–76.

Comiso, J. C., and R. Kwok (1996), The summer Arctic sea ice cover from satellite observations, *J. Geophys. Res.*, *101*, 28,397–28,416.

Comiso, J. C., D. J. Cavalieri, and T. Markus (2003), Sea ice concentration, ice temperature, and snow depth, using AMSR-E data, *IEEE Trans. Geosci. Remote Sens.*, *41*, 243–252.

Eicken, H., M. A. Lange, and G. S. Dieckmann (1991), Spatial variability of sea-ice properties in the northwestern Weddell Sea, *J. Geophys. Res.*, *96*, 10,603–10,615.

Grenfell, T. C. (1992), Surface-based passive microwave studies of multi-year ice, *J. Geophys. Res.*, *97*, 3485–3501.

Jacobs, S. S., and J. C. Comiso (1997), Climate variability in the Amundsen and Bellingshausen seas, *J. Clim.*, *10*(4), 697–709.

Kumerow, C. (1993), On the accuracy of the Eddington approximation for radiative transfer in the microwave frequencies, *J. Geophys. Res.*, *98*, 2757–2765.

Markus, T., and D. J. Cavalieri (2000), An enhancement of the NASA team sea ice algorithm, *IEEE Trans. Geosci. Remote Sens.*, *38*, 1387–1398.

Overland, J. E. (2005), The Arctic climate paradox: The recent decrease of the Arctic Oscillation, *Geophys. Res. Lett.*, *32*, L06701, doi:10.1029/2004GL021752.

Parkinson, C. L., J. C. Comiso, H. J. Zwally, D. J. Cavalieri, P. Gloersen, and W. J. Campbell (1987), Arctic sea ice 1973–1976 from satellite passive microwave observations, *NASA Spec. Publ.*, *489*, 296 pp.

Parkinson, C. L., D. J. Cavalieri, P. Gloersen, H. J. Zwally, and J. C. Comiso (1999), Arctic sea ice extents, areas, and trends, 1978–1996, *J. Geophys. Res.*, *104*, 20,837–20,856.

Serreze, M. C., et al. (2000), Observational evidence of recent change in the northern high-latitude environment, *Clim. Change*, *46*, 159–207.

Stroeve, J. C., M. C. Serreze, F. Fetterer, T. Arbetter, M. Meier, J. Maslanik, and K. Knowles (2004), Tracking the Arctic's shrinking ice cover: Another extreme September minimum in 2004, *Geophys. Res. Lett.*, *32*, L04501, doi:10.1029/2004GL021810.

Svendsen, E., K. Kloster, B. Farelly, O. M. Johannessen, J. A. Johanessen, W. J. Campbell, P. Gloersen, D. Cavalieri, and C. Matzler (1983), Norwegian remote sensing experiment: Evaluation of the Nimbus 7 Scanning Microwave Radiometer for sea ice research, *J. Geophys. Res.*, *88*, 2755–2769.

Swift, C. T., L. S. Fedor, and R. O. Ramseier (1985), An algorithm to measure sea ice concentration with microwave radiometers, *J. Geophys. Res.*, *90*, 1087–1099.

Tucker, W. B., D. K. Perovich, and A. J. Gow (1992), Physical properties of sea ice relevant to remote sensing, in *Microwave Remote Sensing of Sea Ice*, *Geophys. Monogr. Ser.*, vol. 68, edited by F. Carsey, chap. 2, pp. 9–28, AGU, Washington, D. C.

Vant, M. R., R. B. Gray, R. O. Ramseier, and V. Makios (1974), Dielectric properties of fresh and sea ice at 10 and 35 GHz, *J. Appl. Phys.*, *45*(11), 4712–4717.

Weeks, W. F., and S. F. Ackley (1986), The growth, structure and properties of sea ice, in *The Geophysics of Sea Ice*, *NATO ASI Ser. B*, vol. 146, edited by N. Unterstiener, pp. 9–164, Plenum, New York.

Worby, A. P., and J. C. Comiso (2004), Studies of Antarctic sea ice edge and ice extent from satellite and ship observations, *Remote Sens. Environ.*, *92*(1), 98–111.

Zwally, H. J., J. C. Comiso, C. L. Parkinson, W. J. Campbell, F. D. Carsey, and P. Gloersen (1983), Antarctic sea ice 1973–1976 from satellite passive microwave observations, *NASA Spec. Publ.*, *459*, 206 pp.

Zwally, H. J., J. C. Comiso, C. Parkinson, D. Cavalieri, and P. Gloersen (2002), Variability of the Antarctic sea ice cover, *J. Geophys. Res.*, *107*(C5), 3041, doi:10.1029/2000JC000733.

J. C. Comiso, Cryospheric Sciences Branch, NASA Goddard Space Flight Center, Code 614.1, Greenbelt, MD 20771, USA. (josefino.c.comiso@nasa.gov)

F. Nishio, Center for Environmental Remote Sensing, Chiba University, 1-33 Yayoi-cho, Chiba City, Japan. (fnishio@cr.chiba-u.ac.jp)